UNIVERSITY OF TURKU

BL LAC OBJECTS - VIEW FROM THE HIGHEST ENERGIES

Vandad Fallah Ramazani

TURUN YLIOPISTON JULKAISUJA - ANNALES UNIVERSITATIS TURKUENSIS
SARJA - SER. A I OSA - TOM. 628
ASTRONOMICA - CHEMICA - PHYSICA - MATHEMATICA | Turku 2020

University of Turku

Faculty of science and engineering
Department of Physics and Astronomy
Astronomy
Doctoral Programme in Physical and Chemical Sciences

Supervised by

Elina Lindfors
Adjunct Professor
FINCA
University of Turku
FI-20014 Turku, Finland

Kari Nilsson
Adjunct Professor
FINCA
University of Turku
FI-20014 Turku, Finland

Reviewed by

Paula Chadwick
Professor
Department of Physics
Durham University
United Kingdom

Jukka Nevalainen
Senior research fellow
Tartu Observatory
Tartu University
Estonia

Opponent

Luigi Foschini
Researcher
National Institute of Astrophysics (INAF)
Brera Astronomical Observatory
Italy

ISBN 0082-7002 (PRINT)
ISBN 978-951-29-8100-7 (PDF)
ISSN 2343-3175 (ONLINE)

Acknowledgements

My PhD and this thesis is part of a much longer journey which started in 2010. One person had a significant role in starting this journey. I would like to thank my best friend, Mehrnoosh, who encouraged me to get out of my comfort-zone and explore the world. I ended up exploring the Universe.

I have been in good hands during my career in astronomy. Elina Lindfors and Kari Nilsson, my supervisors, are two precious human-beings, I cannot express my appreciation enough. There is no intention to write another thesis about how grateful I am (who is going to supervise that?). I also like to thank Dr. Harry Lehto who gave me the opportunity to start my astronomy career and Prof. Jari Kotilainen, who came to the rescue whenever I was being pushed to quit my academic career.

I want to thank all the members of the MAGIC collaboration who built an amazing scientific arena full of enthusiasm. In particular, Julian and Abelardo who patiently answered all of my endless questions about data analysis, Elisa and Cornelia who are my favourite teammates in many of the projects, Martin for teaching me how to operate two monster telescopes, and finally, Massimo with whom I spent very interesting long nights during a Christmas shift observing the VHE gamma-ray sky.

Special thanks to my friends in "Team Sähly"; Mikko, Janne, Pekka, Pekka M., Harri, Esko (also thanks for proofreading), and Pasi. I enjoyed our twice a week exercise sessions. It was not only a place to exercise but also a place to get rid of work stresses (finish it). I like to thank my valuable friends: Fahimeh, Hassan, Armin, Nasrin, Elmira, Kalle, Pauli, Marie, Stanley and many others, with whom I shared my moments during all these years.

I would like to thank my mom, dad, and siblings without whom I can not imagine life. Last but not least, I like to express my gratitude to the love of my life, Mahboobeh, who is always by my side and has unconditionally supported me on my quest.

Contents

Abstract

Relativistic jets launched by a super-massive black holes are among the most extreme particle accelerators in the Universe. BL Lac objects host a relativistic jet that points very close to our line of sight. They are the most numerous sources in the extragalactic very-high-energy (VHE $> 100\,\mathrm{GeV}$) gamma-ray sky and have been suggested to be possible sources of astrophysical neutrinos. Additionally, due to their high brightness, they can be used to study many fundamental problems like the properties of the Universe between us and them. However, in order to do so, we need to know the intrinsic spectrum of many BL Lac objects and the emission mechanisms that cause their variability. In this thesis, some of the long-standing questions about BL Lac objects are addressed using multi-wavelength data.

With the aim of increasing the number of the BL Lac objects in the VHE gamma-ray sky, a prediction method needs to be developed. As an outcome, a candidate list of VHE gamma-ray emitting (TeV) BL Lac objects is provided for further observations. Three of these candidates (S2 0109+22, TXS 0210+515, and 1ES 2037+521) were followed by VHE gamma-ray observations. I performed a detailed study of these three sources. In archival data, they had different classifications. S2 0109+22 was classified as an intermediate synchrotron peaked source, while the other two were identified as extreme high synchrotron peaked source (EHBL) candidates. Only a handful of both have been detected at VHE gamma rays. S2 0109+22 was detected in a flaring state, and during this period the peaks of its spectral energy distribution (SED) moved to higher energies. The two other sources showed no variability and our study confirmed them as EHBLs.

I have also studied the emission models of TeV BL Lac objects. I performed a detailed study of five TeV blazars by applying a two-component model which takes into account the observational constraints in the radio and optical bands. I found that such a model can reproduce the observed SEDs. Unlike one-zone models, the model does not require very low magnetic field strengths and it does not ignore the radio part of the SED.

Tiivistelmä

Supermassiivisten mustien aukkojen tuottamat relativistiset suihkut ovat maailmakaikkeuden voimakkaimpia hiukkaskiihdyttimiä. Niin sanotuissa BL Lac -kohteissa suihku on suuntautunut lähes meitä kohti, jolloin ne havaitaan huomattavasti tavallista kirkkaampina relativististen ilmiöiden takia. Suurin osa ekstragalaktisista korkean energian (VHE $> 100\,\mathrm{GeV}$) lähteistä taivaalla onkin BL Lac -kohteita. Niiden on arveltu myös olevan kosmisten neutriinojen lähteitä. Koska ne ovat hyvin voimakkaita säteilijöitä, niitä voidaan käyttää myös selvittämään maailmankaikkeuden ominaisuuksia meidän ja niiden välillä. Jotta tämä olisi mahdollista, on meidän tunnettava niiden lähettämä säteilyspektri mahdollisimman tarkkaan. Tässä väitöskirjatyössä tarkastellaan joitakin BL Lac -kohteiden perusominaisuuksia käyttäen mahdollisimman laajaa havaintoaineistoa.

Väitöskirjatyössä kehitettiin ensimmäiseksi menetelmä ennustamaan voimakkaimmat BL Lac -kohteet taivaalla erittäin korkeaenergisen gammasäteilyn alueella. Sen jälkeen kolme kohdetta tältä listalta (S2 0109+22, TXS 0210+515 ja 1ES 2037+521) havaittiin VHE -alueella ja kunkin kohteen säteilyspektri määritettiin tarkkaan. Ensimmäinen kohteista, S2 0109+22, luokiteltiin ns. “Intermediate Synchrotron Peaked” (ISP) -kohteeksi, kun taas kaksi muuta varmistuivat “Extreme High Synchrotron Peaked” (EHBL) -kohteiksi. Kumpaakin tyyppiä on tähän asti löydetty vain muutama. Lisäksi havaittiin, että kohde S2 0109+22 oli havaintohetkellä purkaustilassa ja että sen energiaspektri oli siirtynyt korkeammille energioille. Kahden muun kohteen kirkkaus ei muuttunut havaintojakson aikana.

Työssä tutkittiin myös BL Lac -kohteiden säteilymalleja. Viiden kohteen säteilyspektriin sovitettiin malli, joka koostui kahdesta säteilykomponentista. Mallinnuksessa käytettiin hyväksi mm. laajaa havaintoaineistoa radio- ja optisella alueella. Tässä työssä havaittiin, että kaksikomponenttimalli ennustaa säteilyspektrin paremmin kuin yksikomponenttimalli, mm. suihkun magneettikentän ei tarvitse olla erittäin heikko ja säteilyspektrin radio-osa voidaan mallintaa tarkemmin.

List of publications

I **Empirical multi-wavelength prediction method for very high energy gamma-ray emitting BL Lacertae objects**,
V. Fallah Ramazani, E. Lindfors, and K. Nilsson, A&A, **680**, 68 (2017)

II **The broad-band properties of the intermediate synchrotron peaked BL Lac S2 0109+22 from radio to VHE gamma-rays**,
MAGIC Collaboration, ... , *V. Fallah Ramazani*, et al., MNRAS, **480**, 879 (2018)

III **New hard-TeV extreme blazars detected with the MAGIC telescopes**,
V. A. Acciari, ... , *V. Fallah Ramazani*, et al., ApJS, **247**, 16 (2020)

IV **Testing two-component models on very-high-energy gamma-ray emitting BL Lac objects**,
MAGIC Collaboration, ... , *V. Fallah Ramazani*, et al., **Submitted to** A&A, (2020)

Publications not included in the thesis

I **Testing emission models on the extreme blazar 2WHSP J073326.7+515354 detected at very high energies with the MAGIC telescopes,**
MAGIC Collaboration, et al., MNRAS, **490,** 2284 (2019)

II **Measurement of the extragalactic background light using MAGIC and Fermi-LAT gamma-ray observations of blazars up to z = 1,**
Acciari, V. A., et al., MNRAS, **486,** 4233 (2019)

III **A fast, very-high-energy γ-ray flare from BL Lacertae during a period of multi-wavelength activity in June 2015,**
MAGIC Collaboration, et al., A&A, **623,** A175 (2019)

IV **Detection of persistent VHE gamma-ray emission from PKS 1510-089 by the MAGIC telescopes during low states between 2012 and 2017,**
MAGIC Collaboration, et al., A&A, **619,** A159 (2018)

V **Multi-wavelength characterization of the blazar S5 0716+714 during an unprecedented outburst phase,**
MAGIC Collaboration, et al., A&A, **619,** A45 (2018)

VI **Detection of the blazar S4 0954+65 at very-high-energy with the MAGIC telescopes during an exceptionally high optical state,**
MAGIC Collaboration, et al., A&A, **617,** A30 (2018)

VII Multiwavelength observations of a VHE gamma-ray flare from PKS 1510-089 in 2015,
Ahnen, M. L., et al., A&A, **603,** A29 (2017)

VIII Optical polarization of high-energy BL Lacertae objects,
Hovatta, T., et al., A&A, **596,** A78 (2016)

IX Optical and radio variability of the northern VHE gamma-ray emitting BL Lacertae objects,
Lindfors, E., et al., A&A, **593,** A98 (2016)

List of abbreviations

AGN - Active Galactic Nuclei
BL Lac - BL Lacertae
CTA - Cherenkov Telescope Array
EBL - Extragalactic Background Light
EHBL - Extremely High-synchrotron-peaked BL Lac
EVPA - Electric Vector Position Angle
FoV - Field of View
FSRQ - Flat Spectrum Radio Quasars
HE - High Energy
HSP - High-synchrotron-peaked BL Lac
IM - Imaginge mode
KAIT - Katzman Automatic Imaging Telescope
IACT - Imaging Atmospheric Cherenkov Telescope
ISP - Intermediate-synchrotron-peaked BL Lac
KVA - Kunglinga Vetenskapsakademi
LAT - Large Area Telescope
LSP - Low-synchrotron-peaked BL Lac
NuSTAR - Nuclear Spectroscopic Telescope Array
MWL - multi-wavelength
MAGIC - Major Atmospheric Gamma Imaging Cherenkov
MOJAVE - Monitoring Of Jets in Active galactic nuclei with VLBA Experiments
MWL - Multi-wavelength
PD - Photo-diode mode
PC - Photon Counting mode SED - Spectral Energy Distribution
SSC - Synchrotron Self-Compton
TeV - VHE gamma-ray emitting
ToO - Target of Opportunity
VHE - Very High Energy
VLBI - Very Long Baseline Interferometry
WT- Windowed Timing mode
XRT - X-ray telescope

Chapter 1

Introduction

Astrophysical jets are streams of magnetised plasma which are thought to be formed in the vicinity of dense astronomical objects (e.g. neutron stars and super massive black holes) or as the results of astrophysical explosions (e.g. Gamma-ray bursts). The detection of astrophysical jets dates back to 1918 when Curtis (1918) detected "a curious straight ray..." in the optical image of object Messier 87. Rees (1966) suggested the existence of relativistic motion (with a velocity near to the speed of light) in astrophysical jets in order explain the fast variability of radio sources, such as 3C 273. The relativistic jets of Messier 87 and 3C 273 are among the most famous astrophysical jets and they are launched by the accretion of matter to super-massive black holes in the centre of distant galaxies. Such galaxies are called Active Galactic Nuclei (AGN).

Relativistic jets launched by super-massive black holes (together with PeVatrons and Pulsar winds) are among the most extreme particle accelerators in the Universe. They shine bright in all energy bands from radio to very-high-energy (VHE: $E > 100\,\mathrm{GeV}$) gamma rays. Almost all of the extragalactic sources, which are detected at the highest photon energies (i.e. gamma rays), host relativistic jets. In blazar-type AGN the relativistic jet points very close to our line of sight. BL Lacertae (BL Lac) objects, the objects studied in this thesis, are a sub-class of blazars. BL Lac objects are the most numerous extragalactic sources to be detected at VHE gamma rays.

VHE gamma-ray astronomy, together with cosmic ray physics, neutrino astronomy, and gravitational wave physics form the so called multi-messenger astronomy. The phenomenon that accelerates particles to energies that can emit VHE gamma rays, can also accelerate protons (i.e. ultra high energy cosmic rays) that can then produce ultra high energy neutrinos.

BL Lac objects can be multi-messenger sources. Recently the IceCube Neutrino Observatory (IceCube) and the Major Atmospheric Gamma Imaging Cherenkov (MAGIC) telescopes have announced a VHE gamma-ray flaring activity from a BL Lac object that is coincident with the direction of ultra high energy neutrino observed by IceCube (IceCube Collaboration et al., 2018; Ansoldi et al., 2018). This is a hint that BL Lac objects could be the sources of astrophysical neutrinos. However, the level of significance of the association is still under debate (see e.g. Luo & Zhang, 2020).

The year 2019 marked the 30^{th} birthday of the clear detection of VHE gamma-ray emission using ground-based Imaging Atmospheric Cherenkov Telescopes (IACTs). In 1989, the Crab Nebula was discovered as the first detected object in VHE gamma-ray band (Weekes et al., 1989). By the end of 2004, only 22 objects had been added to the list. The number of VHE gamma-ray emitting (TeV) objects has increased dramatically by a factor of 10 since 2005. The total number of the TeV sources is now 227, from which 84 sources are extragalactic. With the exception of four sources in Large Magellanic Cloud (H. E. S. S. Collaboration et al., 2015a; Komin et al., 2017, 2012), three gamma-ray bursts (MAGIC Collaboration et al., 2019; Abdalla et al., 2019; De Naurois, 2019), and two starburst galaxies (Acero et al., 2009; VERITAS Collaboration et al., 2009), all extragalactic TeV objects are AGN. BL Lac objects are the the most numerous sources (>80%) among TeV AGN (TeVCAT online catalogue Wakely & Horan, 2008).

The VHE gamma-ray observations of BL Lac objects allow us to study particle acceleration, cooling, and the emission mechanisms in the highest energies. Additionally, the VHE gamma-ray emission from BL Lac objects does not travel the Universe unaffected. The VHE gamma-ray photons can produce electron-positron pairs with the photons of the extragalactic background light (EBL), the accumulated light emitted by all stars and galaxies in the Universe. Therefore, the VHE gamma-ray spectra of the distant BL Lac objects measured on earth can be used to study the level and spectrum of the EBL. However, in order to do so, we need to better understand BL Lac objects. In particular, we need to know the intrinsic spectrum of BL Lac objects and mechanisms that cause their variability.

The observed emission of BL Lac objects is dominated by the non-thermal emission of their relativistic jets and can be described as a continuous spectral energy distribution (SED), spanning from radio to VHE gamma-ray frequencies (Fig. 1.1), featuring two wide peaks (e.g. Ghisellini

et al., 2017). The frequency of the lower energy peak, which is located between infra-red and X-ray bands, is used to divide BL Lac objects into sub-classes. These sub-classes are low, intermediate, and high synchrotron peaked (LSP, ISP, and HSP) sources (Abdo et al., 2010c). Moreover, it is evident that there are BL Lac objects with their low-energy peak frequency exceeding the soft X-ray band. Costamante et al. (2001), defined these objects as extreme high-frequency-peaked BL Lac objects (EHBLs).

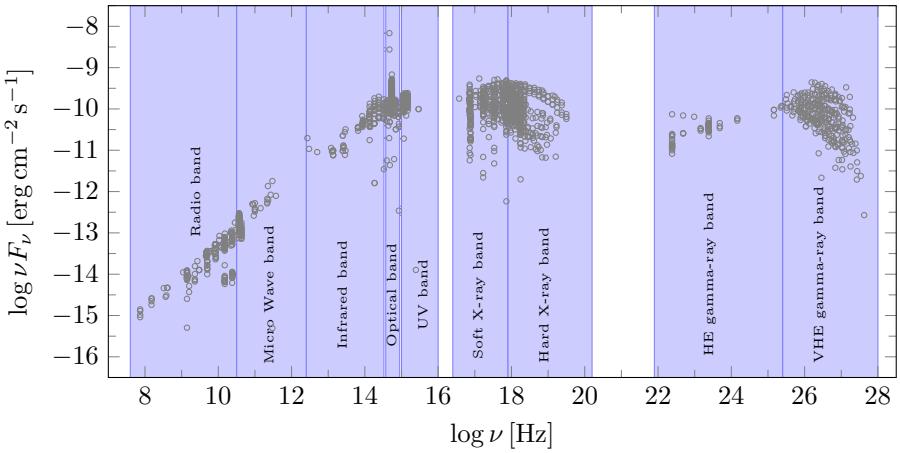

Figure 1.1: An example of the observed spectral energy distribution of a blazar, showing the typical two bump structure. Blazar Mrk421 is one of the most observed blazars. The data points are obtained from the ASI Space Science Data Centre.

The current population of VHE gamma-ray detected (TeV) BL Lac objects represents only the tip of the iceberg of the whole blazar population that contains many peculiar objects. Traditionally the searches for new VHE gamma-ray BL Lac objects were focused on HSP BL Lac objects, which were considered to be the best candidates for VHE gamma-ray emission, but recent discoveries have shown that sources from all BL Lac sub-classes emit VHE gamma rays (e.g. H. E. S. S. Collaboration et al., 2015b; MAGIC Collaboration et al., 2018b).

MAGIC telescopes have discovered over 34 extragalactic VHE gamma-ray emitters, most of which are blazars. The majority of these discoveries

have been made through Target of Opportunity (ToO) observations (e.g. Lindfors & MAGIC Collaboration, 2012; Ahnen et al., 2016b, and references therein). These discoveries have revealed the most distant VHE gamma-ray blazars (Ahnen et al., 2015), but also blazars of unexpected types, (i.e. non-HSP BL Lac objects). While MAGIC has constantly been improving its low energy sensitivity (Aleksić et al., 2016), which also increases its discovery potential, the real leap in the number of TeV blazars will come when Cherenkov Telescope Array (CTA) goes online.

Hassan et al. (2017) found that the number of detectable blazars at VHE gamma rays by CTA will be at least 500, based on simulations using the high-energy gamma-ray data collected by the Large Area Telescope (LAT) on-board of *Fermi Gamma-Ray Space Telescope* (*Fermi*) (Ajello et al., 2017). However, the number can be significantly larger as there might be populations (for example low luminosity EHBLs), that are beyond the reach of *Fermi*-LAT sensitivity. In the current pre-CTA era, further discoveries are still very valuable to improve the statistics of the TeV blazar population.

The first goal of my thesis was to understand what makes a blazar emit gamma rays and provide tools for MAGIC and CTA to discover more VHE blazars in the most efficient way. In other words, my goal was to introduce a list of the best TeV BL Lac candidates for targeted observations. The second goal of my thesis was to increase the number of non-HSP TeV BL Lac objects using the candidate list from the previous step. Finally, I have been investigating if the observationally-constrained two-component model can reproduce the broadband properties of TeV BL Lacs better than the traditional one-zone SSC model.

Chapter 2

Blazars

AGN are exceptionally luminous compared to normal galaxies in all parts of the electromagnetic spectrum. The radiation from AGN is believed to be a result of the accretion of matter by a super-massive black hole at the centre of a host galaxy. They are the most luminous persistent sources of electromagnetic radiation in the Universe. Being very bright and abundant at high redshifts, AGN can be used to study the distant Universe. Blazars constitute a subclass of AGN, with jet axes oriented close to the observer's line of sight (Fig. 2.1). They are divided into two sub-classes, flat spectrum radio quasars (FSRQs) and BL Lac objects. FSRQs are observationally characterised by broad spectral lines in the optical band, while such lines are weak or not present in BL Lac objects. The emission from the jet outshines the emission from the other components of the blazar (e.g. accretion disk and dusty torus). The jet emission is a result of synchrotron emission in frequency ranges below 10^{18} Hz. Relativistic beaming in blazar jets gives rise to their distinctive observational features, such as superluminal motion, rapid variability, and high polarisation.

The blazar jet can be spatially resolved in radio to millimetre wavelengths. This can be achieved through very-long baseline interferometry (VLBI, see e.g. Piner & Edwards, 2004; Piner et al., 2008, 2010; Tiet et al., 2012; Pushkarev et al., 2012; Piner & Edwards, 2018; Lister et al., 2019). In this method, multiple telescopes simultaneously observe same target, forming an interferometer. The angular resolution (typically between a microarcsecond to some milliarcseconds) depends on the observing frequency and the distance between the telescopes. The output images of VLBI observations usually show narrow one-sided jets, and its brightest component is called the core. Many of the jets also show moving knots which are interpreted as shocks propagating in the jet plasma. The plasma in the jet is

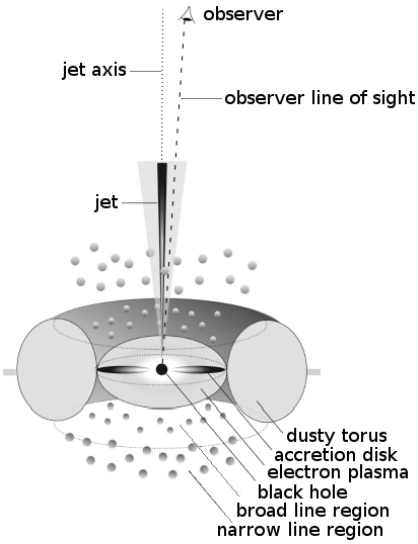

Figure 2.1: Schematic of blazar structure (Adopted from Beckmann & Shrader, 2012).

moving with velocities near the speed of light. Therefore, the light emitted by the knots precedes the knots themselves only slightly, which leads to the phenomenon of superluminal motion. This was seen for first time in the jet of 3C 273 (Rees, 1966; Cohen et al., 1971; Pearson et al., 1981). Nowadays, VLBI observations are routinely used to measure jet speeds, magnetic field strengths, and to resolve the topology of AGN jets (e.g. Boston university monitoring program Jorstad & Marscher, 2016 and Monitoring Of Jets in Active galactic nuclei with VLBA Experiments (MOJAVE) programme Lister et al., 2018, see also Sec. 3.2.5).

The radiation from blazars show variability in all wavelengths (radio: Hughes, 1965; optical: Schmidt, 1963; X-ray: Schreier et al., 1982; gamma rays: Bignami et al., 1981). These variations have timescales ranging from a few minutes to years. In the optical and radio bands, the observed variability is the result of shock propagation in the jet (Marscher & Gear, 1985; Hughes et al., 1989). In X-rays and gamma rays, the variability in the timescales longer than several hours can also be described by the shocks-in-the-jet model. However, it is difficult to explain the fast variability (with

timescales shorter than several hours) using the shock acceleration models. During episodes of fast variability, a compact region of the blazar jet outshines the rest of the jet and more complicated models, such as magnetic re-connection, should be considered (Petropoulou et al., 2016). Traditionally, the variability timescale is used for constraining the size of the emission region via the causality relation, $R < ct_{var}\delta/(1+z)$. In order to study the variability of the blazars, multi-wavelength (MWL) data observed over multiple years with cadence as short as few minutes obtained by sensitive instruments would be desirable (see Sec. 3.2).

Variability is sometimes correlated between two bands (e.g. radio and optical, Lindfors et al., 2016). The long-term variability of blazars has been extensively studied in radio and optical bands. However, since the beginning of the *Fermi*-era such studies have been extended to higher energies (Max-Moerbeck et al., 2014b). Many MWL observation campaigns in the X-ray and VHE gamma-ray bands revealed that there is a correlation between these two bands (Acciari et al., 2011; Aleksić et al., 2015; MAGIC collaboration et al., 2020). These correlations can be used to probe the similarity and connection of the emission regions that are responsible for the radiation in different bands (Sec. 3.4).

Being the result of synchrotron emission, the observed emission from blazars is polarised. Currently, polarised radiation of blazars is only detectable in radio and optical bands due to technological restrictions. In blazars, the fraction of the radiation which is polarised (the polarisation degree) can reach 40% in the optical band. Similar to the total flux, the observed polarisation is also variable both in terms of polarisation degree and direction of electric vector position angle (EVPA) (see e.g. Böttcher, 2019 and references therein).

While the polarisation studies of blazars date back to the 1980's (Valtaoja et al., 1989, and references therein), the optical polarisation of TeV BL Lac objects has been poorly studied until very recently. A first systematic study (Hovatta et al., 2016) showed that there is no difference between TeV and non-TeV BL Lac objects and that also TeV BL Lac objects show the rotation of the EVPA. These rotations, even if we do not yet fully understand their physical origin, can be used to locate the emission region within the jet of BL Lac objects. Comparing these rotations with data obtained from VLBI in the radio band, we can also constrain the strength of the magnetic field. It is a crucial parameter for discriminating the efficiency of leptonic and hadronic processes in the BL Lac jet, i.e. to judge

whether the jet can really produce ultra high energy neutrinos. In order to understand the polarisation behaviour of TeV BL Lac objects, we used two different analysis method in this thesis (Sec. 3.5).

The SED of the blazars show a two-bump structure. The low-energy SED bump, has its maximum located in the frequency range from infra-red to X-rays, is thought to be the synchrotron emission of particles spiralling in the magnetic field of the jet. The physical origin of the high-energy SED bump, with its maximum located in the frequency range from X-ray to VHE gamma-ray bands, is commonly attributed to inverse Compton (IC) scattering of low-energy photons (Rees, 1967). The low-energy photons can be produced within the jet via synchrotron emission (synchrotron self-Compton scattering, SSC, Konigl, 1981; Maraschi et al., 1992) or originate from an external field other than the jet (external Compton scattering, Dermer & Schlickeiser, 1993).

In BL Lac objects, there is no observational evidence confirming the presence of strong external photon fields. Therefore, the seed photons for Compton scattering must originate from the synchrotron emission. Consequently, single-zone SSC models have been used to describe the SED of BL Lac objects (Bloom & Marscher, 1996; Tavecchio et al., 1998). However, there is growing evidence that this model does not reproduce all the observed features of BL Lac objects (Aleksić et al., 2014; Tavecchio & Ghisellini, 2016; Cerruti et al., 2017) and more complicated models should be considered.

Alternatively, it is possible to explain the high-energy emission as a result of the acceleration of hadrons along with leptons in the jet (Mannheim & Biermann, 1989). The accelerated hadrons can produce ultra high energy neutrinos via proton synchrotron emission (Mannheim, 1996; Aharonian, 2000; Mücke & Protheroe, 2001) or photo-pion production and its higher order processes with multi-pion production (Aliu et al., 2014; Dermer et al., 2014). The product of these processes are e.g. charged and neutral pions. The neutral pions decay and produce gamma rays. The charged pion and muon decay will produce relativistic neutrinos, electrons, and positrons. The detection of an ultra high energy neutrino in the direction of a flaring BL Lac object (IceCube Collaboration et al., 2018) gave further impetus to the usage of hadronic models in order to explain both electromagnetic emission and the detection of ultra high energy cosmic rays (see e.g. Ansoldi et al., 2018; Cerruti, 2019; Moharana et al., 2020; Cao et al., 2019).

As it is still an open question which of the emission models describe the

SED of blazars more accurately, in this thesis, many different models have been tested. In particular, a spherical single-zone SSC model and a two co-spatial components model (details in Sec. 3.6) were used to reproduce the SED of the TeV BL Lac objects in Paper II and Paper IV, respectively. Moreover, a conical one-zone SSC model (Asano & Hayashida, 2018), a two-zone spine-layer SSC model (Tavecchio & Ghisellini, 2008), and a proton synchrotron model (Cerruti et al., 2015) were used to study the broadband SED of Extreme BL Lac objects by the author's collaborators (Paper III). In addition to the SED studies, I have also studied the other distinctive features of blazars, the variability and the polarisation behaviour of blazars, as discussed in next sections.

Chapter 3

Samples, data, and analysis methods

As discussed in previous sections, the emission from the blazars is observable in a wide range of the electromagnetic spectrum from radio to VHE gamma-ray frequencies. Therefore, MWL observations play an important role in understanding the physics behind the blazar phenomenon. In this section, the samples, observational data, and the analysis methods used in the thesis are introduced.

3.1 Samples

In Paper I, two samples of BL Lac objects were used (a TeV sample and a non-TeV sample). By the end of 2015, there were 55 sources which were classified as a BL Lac object in the online catalogue for VHE gamma-ray astronomy (TeVCat Wakely & Horan, 2008). There were two sources with uncertain classification (IC310 and HESS J1943+213). Moreover, the VHE gamma-ray spectral properties of six sources were not published by the end of 2015. Therefore, a sample of 47 TeV BL Lac objects was formed to investigate the correlation between different pairs of energy bands and to build the prediction method. Furthermore, a sample of 182 non-TeV BL Lac objects with then known redshifts were selected based on the availability of MWL data in at least three bands out of Radio (4.85 GHz) , mid-IR, Optical (R-band), X-ray (2-10 keV), and HE gamma-ray (1-100 GeV). We searched for promising TeV candidates in the non-TeV sample using an empirical prediction method (Sec.3.3).

Paper II was devoted to study a single source which was listed as a promising TeV candidate in Paper I. We used part of the TeV sample described in Paper I to compare the flux of S2 0109+22 with the multiple-detected TeV BL Lac objects at VHE gamma rays. In Paper III, aiming at detection of TeV EHBLS, different approaches have been used to select the EHBL targets for VHE gamma-ray observation. Five different criteria are applied to the pre-selection of the sources:

i) Based on the definition of EHBL sources, the synchrotron peak of the candidates are expected to be located at frequencies above 10^{17} Hz (Abdo et al., 2010b). Therefore, the X-ray spectral index of the candidates should be below 2.0.

ii) The spectral index of the HE gamma-ray spectrum of the objects should be below 2.0.

iii) X-ray to radio flux ratio should be large (Bonnoli et al., 2015).

iv) From the candidates introduced in Paper I, those which follow criteria (i) and (ii), i.e. TXS 0210+515 and 1ES 2037+521, were selected for VHE gamma-ray observations.

v) The sources with lower redshift are favoured in our sample.

In summary, 10 objects were selected for VHE gamma-ray observations together with 1ES 0229+229 which is the prototype of an EHBL.

In Paper IV, we studied a sample of five TeV BL Lac objects that were selected based on their radio and optical variability. Aleksić et al. (2014) used a long-term radio and optical light curve analysis to constrain the two-component SSC models and reproduce the broadband SED of PKS 1424+240. Later, in 2016, similar radio-optical behaviour were found in the light curves of an additional 12 TeV BL Lac objects, among a sample of 32 northern sky TeV BL Lac objects. These sources were showing an increasing/decreasing trend in both the radio (15 GHz) and the optical (R-band) light curves (Lindfors et al., 2016). We selected five of these objects based on the availability of optical polarisation and VHE gamma-ray data. In Paper IV, the MWL long-term light curve of VER J0521+211, PKS 1424+240, 1ES 1727+502, 1ES 1959+650, and 1ES 2344+514 were studied. Moreover, using the additional constrains from VLBI observations, we tested whether two-component models can reproduce the broadband SED of these five sources.

3.2 Data

3.2.1 Optical light curves

A major fraction of optical data used in this thesis was obtained by the Tuorla blazar monitoring program[1]. The program was started in September 2002 to study TeV blazar candidates. Its original aim was to support the VHE gamma-ray observations of MAGIC telescopes (Takalo et al., 2008). Multiple telescopes have been used within the Tuorla blazar monitoring program during the last 17 years (Tab. 3.1). More than 90% of the observations were carried out by a 35 cm Celestron attached to the Kunglinga Vetenskapsakademi (KVA) telescope. In total, 19145 data points (i.e. optical flux measurements) were extracted from the Tuorla blazar monitoring program. Each data point was calculated using 3 to 8 (R-band) optical images depending on the brightness of the source. The images were processed using a semi-automatic pipeline based on a differential photometry method. The method and full description of data analysis procedure are described in Nilsson et al. (2018).

In Paper I, the majority of the optical measurements were obtained from Tuorla blazar monitoring program with some additional optical data points collected from an all-sky optical catalogue of radio/X-ray sources (Flesch & Hardcastle, 2004) and the 6dF galaxy survey (Jones et al., 2009). The source studied in Paper II (S2 0109+22) was added to the Tuorla blazar monitoring program in 2015. Therefore, the long-term optical light curve was constructed using additional data from the 76-cm Katzman Automatic Imaging Telescope (KAIT) at Lick Observatory (Li et al., 2003) and the Catalina Real-Time Transient Survey (Drake et al., 2009). The KAIT and Catalina data were obtained from unfiltered observations, whose effective colour is close to the R-band. The overall light curve has the time span of > 11 years, between December 4^{th}, 2005 (MJD 53708), and February 16^{th}, 2017 (MJD 57800). The light curve obtained by KAIT overlaps with those obtained from the other two programmes. Using the data points obtained during these two overlapping periods and implementing similar procedure described by Nilsson et al. (2018), we searched for systematic offsets between the light curves. We found that once the data were corrected for galactic extinction, the systematic differences between the telescopes were lower than the statistical uncertainties associated with the observations.

[1] http://users.utu.fi/kani/1m/

Table 3.1: Telescopes used in the Tuorla blazar monitoring program.

Telescope	Mirror size (cm)	Location
Tuorla	103	Piikkiö, Finland
KVA	35	La Palma, Canary Islands
PNM	40	New Mexico, USA
BEL	60	Belogradchik, Bulgaria
ACU	50	San Pedro de Atacama, Chile
NOT	256	La Palma, Canary Islands

In Paper IV, the optical data of the five sources in the sample was obtained from the Tuorla blazar monitoring programme between MJD 56200 (September 30$^{\text{th}}$, 2012) and 58320 (July 21$^{\text{st}}$, 2018). All of the optical measurements are corrected for Galactic extinction and the contribution of the host galaxy in the optical data is subtracted, when applicable.

3.2.2 Optical polarisation

In 2014, a multi year monitoring program was proposed to the Nordic Optical Telescope (NOT) to study the polarisation behaviour of often neglected sources from polarisation study samples (TeV BL Lac objects). Weekly observations were carried out using the ALFOSC[2] instrument with the standard linear polarisation set-up (lambda/2 retarder followed by calcite) in the R-band between 2014 and 2018. The observations were conducted under good sky conditions (seeing ~ 1").

The sky subtracted source counts of the ordinary and extraordinary beams were measured using a standard aperture photometry procedure. The ratios of the measured counts between the two beams were used to calculate the normalised Stokes parameters, the polarisation fraction, and the EVPA for each observation Landi Degl'Innocenti et al. (2007). The instrumental systematic polarisation uncertainty was continuously monitored by additional monthly observations of multiple standard stars. It was found that these systematic uncertainties are negligible compared to the statis-

[2] http://www.not.iac.es/instruments/alfosc

tical uncertainties of the observations. The details of the analysis method are described in Hovatta et al. (2016) and Paper II.

In total, 53 TeV BL Lac objects were monitored for 3 to 6 years. The total of 362 data points for six sources were used to study the polarisation behaviour of the TeV BL lac objects in Paper II and Paper IV. Two different statistical methods were used to interpret these observations (see sec. 3.5).

3.2.3 X-rays

The *Neil Gehrels Swift observatory (Swift)* is a MWL, rapid-response satellite observatory launched on November 20$^{\text{th}}$, 2004, managed by NASA's Goddard Space Flight Centre, and operated by Penn State University. It carries three instruments: a burst alert telescope (BAT, 15-150 keV), a narrow-field X-ray telescope (XRT, 0.2–10 keV), and a UV/optical telescope (UVOT, 170–600 nm). It was originally designed for studying Gamma-ray bursts and their afterglows (Gehrels et al., 2004). However, the total number of point-like objects detected by XRT (Burrows et al., 2004) was 89053 during its first 7 years of observations. Excluding the GRBs, the sources which were affected by bad quality of images, and assuming all entries within 12" (typical positional uncertainty value for faint sources) as one object, the number of distinct sources would be $\sim$ 36000 (D'Elia et al., 2013). Having a flexible observing strategy and the fast reaction capability to target of opportunity requests, *Swift* has been monitoring a list of 176 gamma-ray sources (*Fermi*-LAT sources of interest) most of which are blazars (Stroh & Falcone, 2013). With the exception of the 58 objects in the non-TeV sample of Paper I, all of the objects in the samples described in Section 3.1 were observed by *Swift* multiple times.

The data obtained by *Swift*-XRT in the energy range of 0.3 and 10 keV were processed and analysed to fulfil multi-purpose demands within this thesis. In the following paragraph, the data reduction procedure will be described. The blazar spectrum can be described analytically by either a power law (PL) or log-parabola (LP) function (see e.g. Massaro et al., 2004). They are defined as follows:
a simple power law

$$\frac{dF}{dE} = F_0 \left(\frac{E}{E_0} \right)^{-\Gamma} \tag{3.1}$$

and a log-parabola

$$\frac{dF}{dE} = F_0 \left(\frac{E}{E_0} \right)^{-\Gamma - \beta \times (\log_{10}(E/E_0))}, \tag{3.2}$$

where dF/dE is the differential flux as function of energy (E). F_0, Γ, and β are the flux at the normalisation energy (E_0), the spectral index, and the curvature parameter of the spectrum at E_0.

The XRT has four different operating modes. They are imaging mode (IM), photo-Diode mode (PD), windowed Timing mode (WT), and photon counting mode (PC). The imaging mode is only used to obtain the X-ray position of a new source and no spectral information is stored in their event list. Therefore, the data which is obtained by IM mode were not used in this thesis. The PD mode was a high timing resolution mode and was discontinued in 2005 due to technical issues. The WT mode provides one-dimensional images with 1.8 millisecond time resolution. The images obtained using WT mode appear as a single strip of data which is oriented at the space craft roll angle. In this mode, every ten rows are compressed into a single row and only the 200 columns of field of view (FoV) are read out ($\sim 8'$). Finally, the PC mode is two-dimensional imaging mode with 2.5 second time resolution and cover a region of $24' \times 24'$. Normally, the sources with flux < 1 mCrab are observed using PC mode and the sources with X-ray flux in the range between 1 and 600 mCrab are observed in WT mode (Burrows et al., 2004, 2005).

The flow diagram of the data analysis procedure of XRT is shown in Figure 3.1. Once a source is observed by *Swift*-XRT, the raw data will be transferred to the ground station at the Swift Data Centre at NASA's Goddard Space Flight Centre. The data will then be processed using the xrtpipeline application embedded in the NASA's High Energy Astrophysics Software[3] (HEASoft). During the first two stages, the data is screened, calibrated, cleaned, and all the necessary information is loaded to the level 2 event lists. For our purposes, the level 2 event lists are downloaded from the publicly available SWIFTXRLOG (*Swift*-XRT Instrument Log)[4].The downloaded data are input files of a semi-automatic analysis pipeline (hereafter X-ray pipeline). The X-ray pipeline is developed by the author of this thesis following the standard analysis procedure of *Swift*–XRT data (Evans

[3] https://heasarc.gsfc.nasa.gov/docs/software/heasoft/

[4] https://heasarc.gsfc.nasa.gov/W3Browse/swift/swiftxrlog.html

et al., 2009) and it is designed to produce scientific X-ray products (spectral parameters and the X-ray flux) of multi-epoch observations. For the data obtained in PC mode, the source region is defined as a circle of 20 pixels at the centre of the source, while the background region was defined by a ring centring at source with an inner and outer radius of 40 and 80 pixels (Paper I). For the WT observation data, the source region is defined by a box with a length of 40 pixels at the centre of the source and aligned to the telescope roll angle. A similar box located 100 pixels away from the source position is defined as the background region (Paper III). For both modes

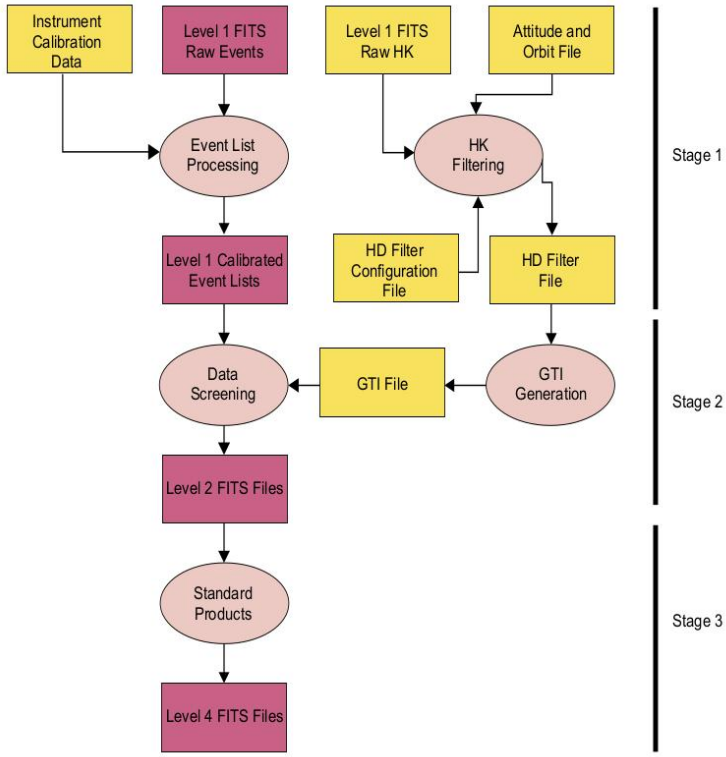

Figure 3.1: The flow diagram of XRT data analysis procedure. Image credit: The *Swift*-XRT Data Reduction Guide (Capalbi et al., 2005).

of observation, due to the open issues for analysing the *Swift*–XRT data[5], we fitted the spectra of each observation using the XSPEC program and assume all possible combinations of pixel-clipping and point-spread-functions together with two mathematical models (i.e. PL and LP), a normalisation energy $E_0 = 0.3\,\mathrm{keV}$, and the fixed equivalent Galactic hydrogen column density reported by Kalberla et al. (2005). In total, for each XRT observation between 6 and 16 spectra (for PC and WT modes, respectively) were extracted and the best-fitted model was selected using the least χ^2 and F-test methods. With the exception of 1ES 2037+521, all of the spectra were fitted in range of 0.3 and 10 keV (see details in Paper III). In total, using the X-ray pipeline, the light curves and time-dependent spectral properties of 50 sources, obtained from 1260 *Swift*–XRT observations, were produced for the purpose of this thesis. Moreover, the X-ray pipeline was used to analyse the data for several other MAGIC collaboration publications not included in the thesis (see page xi). Finally, X-ray data for some targets were collected from the literature to improve the completeness of the data in Paper I.

3.2.4 Very-high-energy gamma rays

MAGIC is a system of two 17 m diameter telescopes located at observatory of Roque de los Muchachos in La Palma, Canary Islands (Spain). It belongs to the third generation of IACTs. The MAGIC telescopes are currently run by an international collaboration of about 165 astronomers from 12 countries. MAGIC is designed to observe gamma rays emitted by galactic and extragalactic objects in the energy range between 50 GeV and 100 TeV. The integral sensitivity ($> 220\,\mathrm{GeV}$), in 50 h of observations, of MAGIC is $(0.66 \pm 0.03)\%$ of the Crab Nebula flux for point-like sources with Crab Nebula-like spectra (Aleksić et al., 2016).

The observations carried out by MAGIC telescopes are used to obtain VHE gamma-ray data in Paper II, Paper III, and Paper IV, while the VHE gamma-ray data in Paper I are collected from literature. The MAGIC collaboration has a dedicated scientific working group for studying AGN

[5]These open issues mostly affect the data obtained with the WT mode. However, some of them (charge traps) still can affect the spectra observed during PC mode. More details are available at:
http://www.swift.ac.uk/analysis/xrt/digest_cal.php and
http://www.swift.ac.uk/analysis/xrt/rmfs.php

Table 3.2: Summary of VHE gamma-ray data analysed by the author of this thesis.

Source name	Publication	Exposure time (h)
S2 0109+22	Paper II	9.6
1ES 2037+521	Paper III	28.1
PKS 1424+240	Paper IV	49.1
1ES 1727+521	Paper IV	6.4
1ES 1959+65	Paper IV	2.5
1ES 2344+514	Paper IV	1.6

which leads multiple observation campaigns. The data used in this thesis are collected as part of different MWL campaigns between 2010 and 2017 with a total integration time of ~ 405 h of good quality data. The author of this thesis, as a member of MAGIC collaboration, analysed $\sim 25\%$ of the used data (Tab. 3.2).

The technical details of indirect VHE gamma-ray observations by MAGIC telescopes are described in Prandini (2011); Schultz (2013); Terzić (2015). The MAGIC observational data is analysed using the MAGIC Standard Analysis Software (MARS, Moralejo et al., 2009; Zanin et al., 2013) taking into account the instrument performance under different observation conditions (Aleksić et al., 2016; Ahnen et al., 2017a). The flow diagram of MAGIC data analysis is shown in Figure 3.2.

In practice, the standard data analysis starts with the data quality check on the output of the `superstar` program, which contains the matching events recorded by the two telescopes and the geometry of the reconstructed shower together with the observation conditions. This process is done with the `quate` program which excludes bad quality data that is caused by clouds, low sky transmission, sky brightness, and/or hardware instability. The second step is to produce matrices which are needed for the background discrimination (a.k.a gamma-hadron separation) and energy reconstruction of the events. These are produced with the `coach` program. The background discrimination uses a multivariate classification analysis based on a Random Forest algorithm (Albert et al., 2008). Random Forest

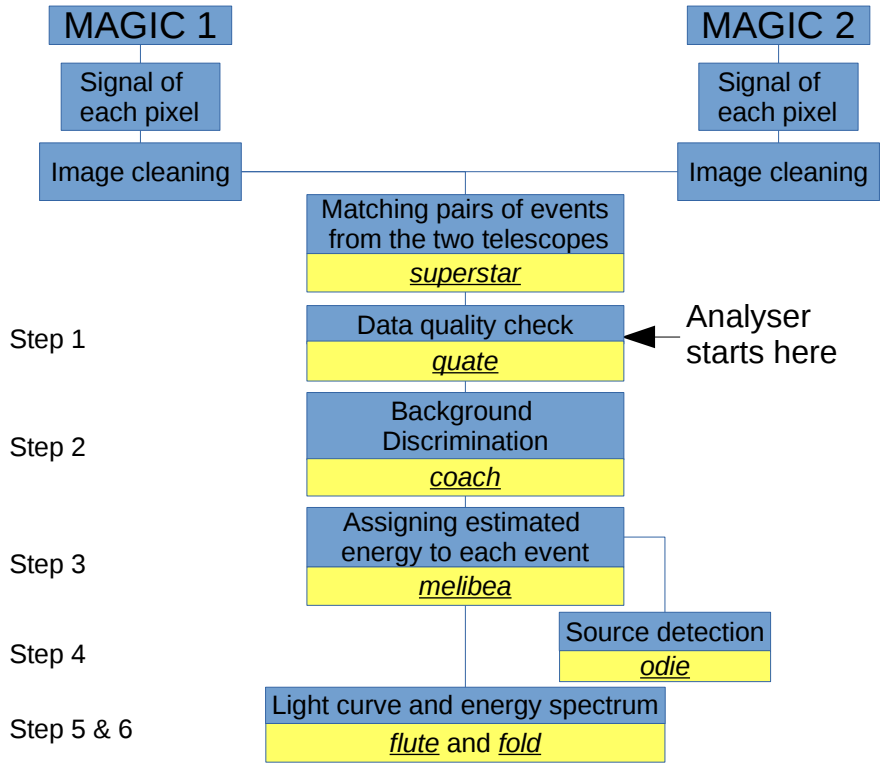

Figure 3.2: The flow diagram of the MAGIC data analysis chain.

is trained on simulated gamma-ray events and hadrons from real observational data (OFF data). The `coach` program also produces look-up tables for energy reconstructions. As for the third step, the matrices are applied to both observational and simulated events via a program named `melibea`. In other words the `melibea` program assigns a *hadronness*[6] and reconstructed energy estimate for each event.

The fourth step of the analysis is the signal search. Data is first cleaned from the events with high *hadroness*, after which the signal search is carried out in the source region by measuring the squared angular distance (θ^2) between the nominal source position in the camera and the reconstructed

[6]Hadronness is the probability of that the event is hadron-like (hadronness=1) or gamma-like (hadronness=0).

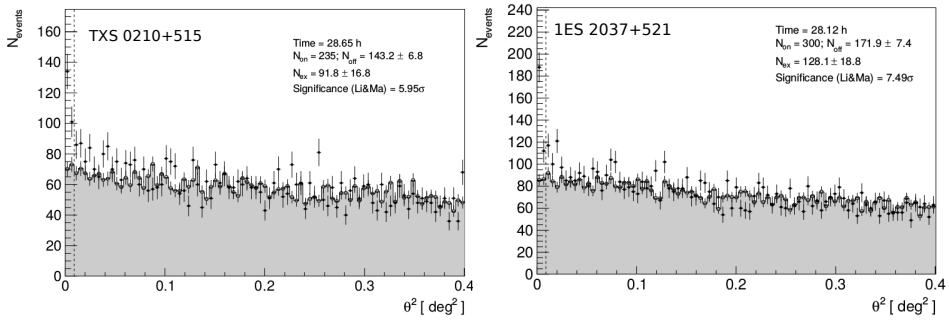

Figure 3.3: Examples of θ^2 plots for two of the sources in Paper III (Left panel: TXS 0210+515, Right panel: 1ES 2037+521). The signal search is performed in the θ^2 region indicated by the vertical dashed line ($\theta^2 \sim 0.01$). The black points show the number of ON events while the grey shaded area show the distribution of the OFF events.

source position in camera coordinates for each event. A similar procedure will be applied to the OFF regions. Then number of excess events is calculated by subtracting the number of events measured in the background control region (OFF region) from the ones in the signal region (ON region). The significance of the signal is then calculated using the method described by Li & Ma (1983). If the significance of the signal is above 5σ, the source is considered as detected in VHE gamma-ray band. Figure 3.3 shows two examples of the θ^2 plot produced as the output of the `odie` program following the description of this step.

The fifth steps consist of calculating the differential spectrum and the light curve of the source. The differential spectrum is defined as follows:

$$\frac{\mathrm{d}N}{dE}(E) = \frac{\mathrm{d}^3 N_{\mathrm{Excess}}}{\mathrm{d}E\ \mathrm{d}A_{\mathrm{eff}}\ \mathrm{d}t_{\mathrm{eff}}}, \tag{3.3}$$

where N_{Excess} is the number of excess events in the energy bin $\mathrm{d}E$ which is calculated based on the description of step four. $\mathrm{d}t_{\mathrm{eff}}$ is the effective observation time. $\mathrm{d}A_{\mathrm{eff}}$ is the effective collection area in which the air shower can be observed by the telescope folded by the detection efficiency[7].

[7]The detection efficiency is estimated from the ratio between the number of simulated gamma-ray showers after applying all of the limits (e.g. hadronness and θ^2) and the total

Integrating equation 3.3 above an arbitrary energy will lead to the integral flux of the source over the observation time. The `flute` program performs all of the calculations described in step 5.

In the sixth and final step, once the spectrum of the source is produced based on the reconstructed energy, the spectral parameters are obtained via forward-folding using a Poissonian maximum likelihood procedure described by Ahnen et al. (2017b). In order to calculate the intrinsic spectral parameters, the same estimation procedure is used by taking into account the source redshift and a proper EBL absorption model. The `fold` program produces the VHE gamma-ray spectrum, applies the EBL absorption correction, and fits a model to the data. As illustrated in Paper I – Paper IV, the VHE gamma-ray spectra of the blazars can be described either with equation 3.1 or equation 3.2.

3.2.5 Other bands

In addition to the data sets described in sections 3.2.1 – 3.2.4, there are other sets of data which were either collected from literature or analysed by collaborators. For the objects in the TeV and non-TeV samples of paper Paper I, the radio fluxes (4.85 GHz) are collected from 87GB, Gregory & Condon (1991); PMN, Griffith et al. (1995); GB6, Gregory et al. (1994, 1996); 1RXS, Voges et al. (1999); and Fossati et al. (1998); Laurent-Muehleisen et al. (1999). Moreover, the mid infra-red fluxes are collected from Wright et al. (2010) and the HE gamma-ray (1-100 GeV) fluxes are collected from the 3FGL catalogue (Acero et al., 2015).

It is evident that there are similarities in the long-term behaviour of blazars at different wavelengths (Lindfors et al., 2016; Hovatta et al., 2014b; Max-Moerbeck et al., 2014b). In order to compare the long-term behaviour of the source S2 0109+22 with a sample of TeV BL Lac objects in Paper II, the radio light curve of the source at 15 GHz and 37 GHz were obtained from the high cadence observations carried out by Owens Valley Radio Observatory (OVRO) 40 m telescope (Richards et al., 2011) and the Metsähovi radio telescope Teräsranta et al. (1998), respectively. The MWL observations, as well as VHE gamma-ray observations were triggered based on the flaring activity of the source in HE gamma rays during July 2015. Therefore, it was important to reconstruct the source spectrum simultaneous to the MWL observations, as its flux differs from the reported values in

number of gamma-ray showers.

catalogues, which generally report time-averaged values over a long period of time. To address this issue, the HE gamma-ray flux and spectrum of the source were analysed from the observations carried out by the *Fermi*–LAT in a period lasting around the three weeks roughly centred on the MAGIC detection. Using the *Fermi*–LAT ScienceTools software package (version v10r0p5), the data reduction of the events of the Pass8 source class was performed in the HE gamma-ray band. In the analysis chain, the un-binned likelihood fit of the data was performed using the suggested Galactic diffuse-emission model and an isotropic component (Acero et al., 2016). The light curve was constructed using 1-day binning and the SED of the source was produced using the data collected between the July 22$^{\rm nd}$, 2015, and July 28$^{\rm th}$, 2015, corresponding to the MAGIC observing period.

High synchrotron peaked sources have the first peak of the SED in a frequency range between the UV and soft X-ray bands (see Sec.1). However, there is evidence that the synchrotron peak frequency of some of the BL Lac objects exceeds the soft X-ray band (Costamante et al., 2001). This opens the so-called EHBL category in the BL Lac classifications. The observations in the hard X-ray band (3-79 keV) are an essential tool to investigate the extremeness of BL Lac objects. In Paper III, we used the hard X-ray spectra of three sources obtained from observations carried out by the Nuclear Spectroscopic Telescope Array (*NuSTAR* Harrison et al., 2013). The spectra were produced by using a joint fit procedure of the simultaneous *Swift*–XRT and *NuSTAR* data for TXS 0210+515 and RGB J2313+147. For 1ES 0229+200, the results are obtained from Costamante et al. (2018). Similar to Paper II, the HE gamma-ray data were extracted from the weekly *Fermi*–LAT data files[8]. The time span for each source varies as a function of source faintness and the MAGIC observation window. The time intervals are minimised in order to have the detection significance for a given source above 5σ confidence level. As the sources in the sample of Paper III are relatively faint in the HE gamma-ray band, the minimum exposure time considered for data analysis of each object was $\sim$ 1 year. The data was analysed using the open-source software package `enrico` (Sanchez & Deil, 2013), for each source in the sample.

In Paper IV, we used the long-term radio (15 GHz) light curve of the sample obtained from the observations performed by OVRO to investi-

[8]Available in the FSSC data centre at: `https://fermi.gsfc.nasa.gov/ssc/data/access/`

gate the long-term behaviour of the sources. Moreover, in order to reduce the number of free parameters of the two-component SED modelling, the constraints of jet parameters were collected from the results of VLBI observations[9] reported by Lister & Homan (2005); Lister et al. (2009, 2016); Hodge et al. (2018); Lister et al. (2019); Piner & Edwards (2004, 2018); Piner et al. (2008, 2010); Tiet et al. (2012). Finally, the HE gamma-ray data were produced using the observations carried out by *Fermi*–LAT. The HE gamma-ray data were analysed with the FermiTools software package (version 11-07-00) and fermipy (version 0.17.4 Wood et al., 2017).

3.3 Empirical multi-wavelength prediction method

To look for new TeV BL Lac candidates, we performed a comprehensive MWL correlation study of the existing TeV BL Lac objects. We then assumed that the same correlations apply for all BL Lac objects and used the correlations to select promising TeV candidates. In this section we describe the approach shortly. The flow chart is shown in Figure 3.4.

In order to implement this approach, ten data sets were formed which contain th k-corrected luminosity of the MWL data of the TeV sample (Paper I). Five of these data sets were based on the average flux of the lower energy bands (i.e. radio, 5 GHz; mid infra-red; optical, R-band; X-rays, 2-10 keV; and HE gamma rays, 1-100 GeV). The VHE gamma-ray data (i.e. integral luminosity above 200) were divided into five categories to reduce the biases arising from the low number of observations in this band and taking into account the variability of the sources. These 10 luminosity data sets formed 35 pairs. In the next step, a non-parametric partial Kendall τ rank correlation test (Akritas & Siebert, 1996) was performed to find the possible correlation between each pair of data sets.

Two models (a linear model, $Y = aX + b$, and a power-law model, $Y = 10^b \times X^a$) were fitted to the 14 pairs of data sets which showed significant correlations using a bi-sectional ordinary least-squared regression method (Isobe et al., 1990). In order to discriminate between two models, the sum of squared residuals was used. The standard bootstrapping method (Efron & Tibshirani, 1993) was implemented to calculate the error bars of the model parameters. Moreover, the dependency of the models on the outliers were tested by comparing the error bars of model parameters obtained

[9] The majority of these observations were carried out within the MOJAVE programme.

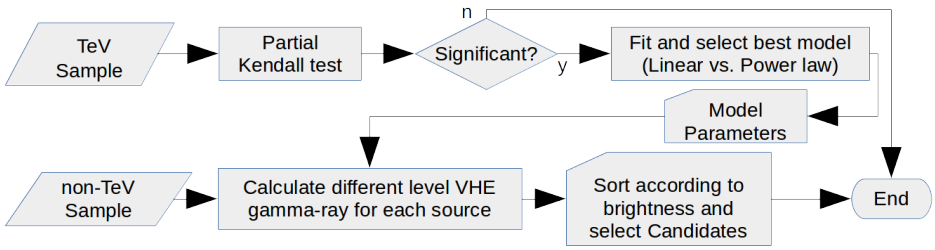

Figure 3.4: Flow diagram of the statistical method for selecting TeV BL Lac object -candidates.

from the bootstrapping method and the ones from the Jackknife method (Efron & Stein, 1981). We found that all of the significant correlations can be described better with the power-law model and were insensitive to the outlier.

As a highlight, the time independent luminosity correlation between optical and VHE gamma-ray bands was, for the first time, established from our analysis. In previous similar works (e.g Costamante & Ghisellini, 2002; Wagner, 2008) this correlation was not significant. Comparing the data sets in the work presented here to those of previous works, we noted the host-galaxy fluxes were not subtracted from the optical fluxes in previous works, and this possibly led to non-significant correlations in these studies.

In total, the VHE gamma-ray band was involved in eight of the flux pairs indicating significant correlation. Based on these eight correlations, we formed our prediction functions, $\log(L_{VHE,pred.}) = b + a\log(L_{R/I/O/X/\gamma})$. These functions used the lower energy luminosity of the non-TeV sample (see sections 3.1 and 3.2) as an input variable and calculated multiple levels of predicted VHE gamma-ray integral luminosity over 200 GeV for each source. At least seven levels of VHE gamma-ray luminosity ($L_{VHE,pred.}$) were calculated for each non-TeV BL Lac object based on the availability of lower energy data for each object. The median of these levels were considered as the predicted level of VHE gamma-ray luminosity.

The predicted VHE gamma-ray flux of the non-TeV sample were calculated using their predicted level of VHE gamma-ray luminosity and redshift. Moreover, a K-correction was applied assuming VHE gamma-ray spectral index of 3.27, which is the average of all the data points in our TeV sample. The non-TeV sample is then sorted based on the median value of

VHE gamma-ray flux of the sources. Comparing the predicted fluxes with the sensitivity of MAGIC telescopes (Aleksić et al., 2016), we found that 53 objects (hereafter TeV BL Lac candidates) in the non-TeV sample are expected to be detectable with current generation IACTs.

The simplistic approach described in Paper I has known caveats which shall be addressed in future works. The objects with unknown redshift were excluded from the population of non-TeV BL Lac objects. Therefore, our search for TeV candidates is restricted to nearby objects. Moreover, BL Lac objects are variable sources. Therefore, the non-simultaneity of the lower energy bands data and the VHE gamma-ray data affected our correlation study. We tried to minimise this effect by considering different states in VHE gamma-ray flux. However, the effect was still present in the lower energy bands. Furthermore, the spectral indices in the HE gamma-ray and the X-ray bands were not taken into account. Therefore, the VHE gamma-ray flux might be overestimated for the sources which have a soft X-ray and HE gamma-ray spectra. Finally, for the sources in the TeV sample, the absorption of VHE gamma-ray emission due to the interaction with the EBL was not taken into account. This was the only viable way not to exclude a large number of sources from the study owing to missing information. It is notable that the majority ($> 70\%$) of the sources in the TeV sample are located at $z < 0.3$, they were detected in the energy range below 500 GeV where the effect of EBL absorption on the integral flux above 200 GeV is relatively small. We expected that this did not bias our results significantly.

3.4 Correlation studies

As discussed in the previous section, cross-band time-independent luminosity correlations were used to build the prediction method and provided a list of TeV candidates. In this section, the analysis methods used to study the temporal behaviour of BL Lac objects is presented. In general, these correlations are used to probe if the emission in different energy bands is causally connected, which can be used as additional constraints in the SED modelling procedure.

Lindfors et al. (2016) studied the long-term optical and radio behaviour of 32 TeV BL Lac objects using data from the OVRO (15 GHz) and Tuorla (optical R-band) blazar monitoring programs. Correlated flares were found

in half of the sources, and correlated long-term trends in 13 sources. Max-Moerbeck et al. (2014b) studied the long-term radio and HE gamma-ray behaviour of 41 blazars using the data from the OVRO (15 GHz) blazar monitoring and *Fermi*-LAT data in the energy range between 100 MeV and 200 GeV. Only three sources show significant correlations at a level larger than 2.25σ, with only one of those larger than 3σ. Both studies (Max-Moerbeck et al., 2014b; Lindfors et al., 2016) used a hybrid method implementing the Power Spectral Density (PSD) analysis (Hufnagel & Bregman, 1992; Max-Moerbeck et al., 2014a) and the Discrete Correlation Function (DCF Edelson & Krolik, 1988). The former was used to simulate the unevenly sampled light curves while the latter was tuned with a local normalisation (LCCF Welsh, 1999) and used to address the irregularly sampled data.

In this work, we extended the study performed by Lindfors et al. (2016) to the then newly discovered TeV BL Lac object (S2 0109+22, Paper II), other wavelengths (37 GHz, Paper II, X-ray, Paper IV), and different observation epochs (2013-2018, Paper IV). The cross-correlation function between different pairs of light curves were calculated using the LCCF function. The temporal binning of the light curves was set to 10 days and the minimum number of elements in each LCCF bin was set to 10. The significance of cross-correlations was estimated using 1000 simulated light curves, which were produced assuming the PSD indices listed in Table 3.3, following the method described by Max-Moerbeck et al. (2014a).

Among 18 tested cross-correlations, only three significant cross-correlations were found in our data sets. They were a radio (15 GHz) – optical correlations of two sources (1ES 1727+502 and 1ES 1959+650) in the sample of Paper IV, and a radio 37 – 15 GHz correlation of S2 0109+22 (Paper II). In all of these three cases, the correlations were rather wide (90, 60, and 40 days for 1ES 1727+502, 1ES 1959+650, and S2 0109+22, respectively) and compatible with zero-days of time lag. Moreover, the significant peaks are rather wide and consistent with zero time lag. These results may indicate the co-spatiality of the emission regions in charge of different bands.

3.5 Polarisation study

The optical emission of blazars is dominated by synchrotron emission. Synchrotron emission is intrinsically polarised and the polarisation fraction can,

Table 3.3: PSD indices used in light curve simulations.

Source name	Radio*		Optical†	X-ray‡
	(15 GHz)	(37 GHz)	(R-band)	(2-10 keV)
S2 0109+22	-1.80	-1.80	-1.50	NA
VER J0521+211	-1.70	NA	-1.60	-1.4
PKS 1424+240	-2.35	NA	-1.54	-1.4
1ES 1727+502	-1.70	NA	-1.40	-1.4
1ES 1959+650	-1.55	NA	-1.70	-1.4
1ES 2344+514	-1.70	NA	-1.47	-1.4

$\star$ Determined from the radio light curves (Max-Moerbeck, private communications).
† Determined from the optical light curves (Nilsson et al., 2018).
‡ Assumed value based on the value reported by Aleksić et al. (2015).

theoretically, reach 70% in optically thin jets with a uniform magnetic field (e.g. Pacholczyk, 1970). In practice, the maximum observed level of fractional polarisation reaches a few tens of percent (e.g. Angel & Stockman, 1980; Angelakis et al., 2016). Moreover, the observed optical polarisation of blazars usually contains signatures of two components: an optical polarisation core and a chaotic component (e.g. Valtaoja et al., 1991; Villforth et al., 2010; Barres de Almeida et al., 2010). In this work, we implemented two different approaches to understand the polarisation behaviour of BL Lac objects. In Paper II, the polarisation variability of S2 0109+22 was quantified and compared to the sample of TeV BL Lac objects. In Paper IV, the polarisation measurements were used to constrain the variable and constant component in the optical band, for the SED modelling.

In the first approach, following the method described by Hovatta et al. (2016), we estimated the long-term polarisation properties of S2 0109+22. In this method the mean intrinsic polarisation fraction, the intrinsic variability amplitude, and their uncertainties were computed using a likelihood approach. The details of the approach are described by Blinov et al. (2016, Appendix A). The EVPA variability of the S2 0109+22 was quantified by calculating its derivative after taking into account the nπ ambiguity. The

polarisation properties were compared to a sample of TeV and non-TeV BL Lac objects. We found that both the intrinsic mean polarisation fraction and its standard deviation over the mean are higher than both TeV and non-TeV samples of BL Lac objects in Hovatta et al. (2016). Moreover, we found that the EVPA median derivative at source frame was 3.3° per day. This showed that the polarisation angle of S2 0109+22 is changing more rapidly than the average value of TeV and non-TeV BL Lac objects (Paper II). This behaviour is in agreement with the ISP classification of the source. In ISP sources, the optical emission probes the peak of the synchrotron component and the variability is expected to be higher (see e.g. Angelakis et al., 2016).

In the second approach (Paper IV, Sec. 3.3 and Appendix C), we followed the idea of separating the relative strengths of the two components (hereafter constant and variable components) from the optical polarisation data. We used a physical model and a Bayesian fitting method instead of the iterative fitting applied by Barres de Almeida et al. (2014). The constant and variable component's contribution in the total Stokes parameters were assumed as follows:

$$\begin{aligned} I &= I_C + I_V \\ Q &= Q_C + Q_V \\ U &= U_C + U_V, \end{aligned} \tag{3.4}$$

where the subscripts C and V refer to the constant and variable components, respectively. The constant component was modelled by letting $I_{\rm C}$, $Q_{\rm C}$ and $U_{\rm C}$ vary. For the variable component, we assumed that the emission is produced by a homogeneous cylindrical emission region in a jet with a helical magnetic field. The Stokes parameters of the variable component were computed using the formulae described by Lyutikov et al. (2005), assuming that the orientation of the variable component remains constant with respect to the observer. In total, the model had 12 parameters. We fixed 5 parameters of the variable component (the index of the electron spectrum, the radius of the emitting region, the length of the emission region, the magnetic field strength, and the apparent speed) to reduce the degree of degeneracy. Therefore, we had 7 free parameters in our model: the Stokes parameters of the constant component, the magnetic field pitch angle, the jet position angle, the viewing angle, and the rms of the turbulence. A Monte Carlo Markov Chain (MCMC) ensemble sampler

(Goodman & Weare, 2010) was used to fit the model to the monochromatic observational data. The posteriori was computed from the Q and U data only.

Our main goal of this approach was to obtain some constraints on the flux ratio of the two emission components in the optical band. Unfortunately, the goal was not achieved in all the cases which were studied in Paper IV. For example, in the case of VER J0521+211 the priori range for I_C was from 0 to 3.0 mJy and the posteriori averages in the middle of this range with errors that fill the priori completely. However, the polarisation study performed here provides limited additional constraints for modelling the SED (Sec. 3.6).

3.6 Spectral energy distribution modelling

The spectral energy distribution is the main tool to study BL Lac objects. As discussed in Chapter 2, there are different models that have been used to reproduce the SED of BL Lac objects. The emission models can differ in emission mechanisms (e.g. leptonic vs. hadronic), but also in the geometry of the emission regions (e.g. spherical blob vs. conical jet).

In Paper II and Paper IV, we applied an emission model that calculates the synchrotron and SSC emission from a spherical emission region. In this model, the emission region is filled with electrons distributed in Lorentz factor according to a smoothed broken power law:

$$N(\gamma) = K\gamma^{-n_1}\left(1+\frac{\gamma}{\gamma_b}\right)^{n_1-n_2}, \gamma_{min} < \gamma < \gamma_{max}. \tag{3.5}$$

The distribution has a normalisation K between γ_{min} and γ_{max} and slopes n_1 and n_2 below and above the break in the electron distribution, γ_b (Maraschi & Tavecchio, 2003). Each of the emission regions has size R, Doppler factor δ and magnetic field strength B.

Traditionally, a spherical single-zone SSC model has been used to describe the broadband SED of the BL Lac objects. In Paper II, we studied the SED of the S2 0109+22 using a single-zone SSC model. In this model, we assumed a small emission region close to the central engine (Fig. 3.5, left) where the radio emission is self-absorbed and, therefore, was neglected from the modelling. The model has eight parameters from which only the minimum Lorentz factor ($\gamma_{\rm min}$) is assumed to be fixed because there is no

instrument available to probe the energy range where its influence would be significant. The results of this SED modelling are discussed in Section 4.3.

Figure 3.5: Sketch of the geometrical SED modelling setup. The emission regions are located several parsecs from the central black hole (at $d_{\rm core}$). *Left:* single-zone spherical SSC model. *Right:* two-components model. Image credit: Elina Lindfors.

In Paper IV, we used a two-component model which was motivated by the results presented in Lindfors et al. (2016) and the successful usage of two-component models by Aleksić et al. (2014). We applied a two-component leptonic model to a sample of eight SEDs of five TeV BL Lac objects. In this model, two interacting co-spatial emission regions (Fig. 3.5, right) are responsible for the observed emission. The two emission regions are called 'core' and 'blob', with sizes $R_{\rm core} > R_{\rm blob}$ and are filled with electrons, whose Lorentz factors are distributed according to a smoothed broken power law (Eq. 3.5).

The number of free parameters in this model is 16. Therefore, we tried to constrain the parameters using observational data as much as possible. The major fraction of the constraints are collected from observational data from the MOJAVE programme (Lister & Homan, 2005; Lister et al., 2009, 2016; Hodge et al., 2018; Lister et al., 2019). Additionally, we collected the results reported by Piner & Edwards (2004, 2018); Piner et al. (2008, 2010); Tiet et al. (2012). These parameters are $R_{\rm core}$, $B_{\rm core}$, and $\delta_{\rm core}$. Moreover, the maximum size of the blob emission region is constrained using the VHE gamma-ray or X-ray variability timescales via the causality relation, $R_{\rm blob} < ct_{var}\delta/(1+z)$. Finally, the strength of the magnetic field

of the blob emission region is assumed to be equal to the one of the core. The rest of the parameters are left as free parameters within physically acceptable ranges (e.g. $K_{blob} > K_{core}$, and $\delta_{blob} < 30$).

Due to the restricted availability of the numerical codes for time-dependent models, all of the observation epochs were modelled independently. The models were tested only on 'snapshot SEDs' and did not include time-evolution. The effect of gamma-gamma absorption between the core seed photon field and the highest energy photons emitted by the blob were found to be negligible. We also tried to take into account the derived estimations of the relative strengths of the core and blob components in the optical, as discussed in the previous sections. The results of this study is discussed in Section 4.3.

Chapter 4

Discussions and conclusions

4.1 TeV BL Lac candidates

As discussed in Section 1, TeV blazars represent a small fraction of blazars. By the end of 2019, only 73 blazars had been detected in the VHE gamma-ray band. Most of these blazars are detected at VHE gamma rays by third generation IACTs (i.e. MAGIC, H.E.S.S. and VERITAS). VHE gamma-ray detection techniques need a relatively long exposure time. Furthermore, no sky survey is available due to the small FoV of the IACT. Therefore, in order to increase the number of TeV blazars, the pre-selection of promising candidates based on lower energy band data is unavoidable. The first systematic works on the pre-selection of extragalactic sources for VHE gamma-ray observation date back to 2002 when the third generation of IACTs were under construction.

The radio, optical, and X-ray properties of 246 BL Lac objects were studied by Costamante & Ghisellini (2002) and 33 TeV BL Lac candidates were introduced based on the similarity of their properties to those of five known TeV BL Lac objects. Massaro et al. (2011) found that the X-ray spectral curvature of the 17 TeV BL Lac objects were systematically lower than those of the 47 non-TeV BL Lac objects. Using the curvature parameter for pre-selection, they proposed 15 TeV BL Lac candidates. Massaro et al. (2013) used the similarity of IR and X-ray properties between the TeV and Non-TeV BL Lac objects to select HSPs for future TeV-observations. D'Abrusco et al. (2014) used the measure of radio-to-IR flux ($q_{22} < -0.5$) to present radio-loud candidates for gamma-ray emitting blazars. Arsioli et al. (1WHSP, 2015) and Chang et al. (2WHSP, 2017) used the ratio between the synchrotron peak flux ($\nu_{peak} F_{\nu_{peak}}$) of a source and the synchrotron peak flux of the faintest TeV blazar to introduce 76 and 136 promising

HSP BL Lac candidates from a list of 992 and 1691 infra-red colour-colour selected sources. Padovani & Giommi (2015) simulated the broadband SED of the 1WHSP sample (taking into account EBL absorption (Domínguez et al., 2011) and typical sensitivity reachable by IACTs $\sim$ 14 mCrab, and $\nu_{\rm synch} > 10^{15}$ Hz) to introduce 70 blazars as TeV candidates.

In Paper I, we presented the most extensive MWL data collection of TeV BL Lac objects, and the first extensive correlation study between low energy and VHE gamma-ray luminosity. There were eight significant correlations with the VHE gamma rays as the second component. These correlations were used to predict VHE gamma-ray flux of 182 non-TeV BL Lac objects. Unlike the methods discussed in the previous paragraph, the method described in Paper I did not include any major physical assumption, such as spectral properties in X-ray and HE gamma-ray bands. Moreover, the variability of the sources was taken into account by using five different VHE gamma-ray data sets (see Sec. 3.3). However, the non-simultaneity of the data sets, ignoring the spectral indices in X-ray and gamma-ray bands, excluding the sources with unknown redshift, and neglecting the EBL absorption effect are the caveats of the empirical prediction method. These caveats should be addressed in future work.

In total, 53 TeV BL Lac candidates were identified based on the median predicted level of VHE gamma-ray flux (see Tab. 4.1 for the 15 most promising candidates). Among them, there are 21 new TeV BL Lac candidates, which were not proposed by any of the above-mentioned methods. One of these newly identified TeV BL Lac candidates was 1ES 2037+521, which is an extreme HSP BL Lac object located at z=0.053 and it was ranked as the ninth most promising candidate. Moreover, TXS 0210+515 was proposed by many of the above-mentioned pre-selection methods (Costamante & Ghisellini, 2002; Massaro et al., 2011, 2013; Chang et al., 2017). It is also an extreme HSP BL Lac object located at z=0.049 and ranked as the fifth most promising TeV candidate in Paper I. Focusing on the less studied class of BL Lac objects (EHBLs), these two objects were proposed for VHE gamma-ray observations by the author of this thesis. The MAGIC telescope performed VHE gamma-ray observations and detected them at VHE gamma rays (Paper III). Furthermore, S2 0109+22 (ranked 42 in the candidate list), which was an ISP with uncertain redshift was detected at VHE gamma rays. The source exhibited a flaring activity in July 2015 and was observed by MAGIC telescopes as a ToO for $\sim$ 10 h at VHE gamma rays. The MAGIC observation led to detection of the source at VHE gamma

rays (Paper II).

In addition to S2 0109+22, TXS 0210+515, and 1ES 2037+521 (to be discussed in Sec. 4.2), four other sources in the non-TeV sample were detected in VHE gamma-ray band during their high state since the formation of the sample in late 2014. They are OJ 287 (Mukherjee & VERITAS Collaboration, 2017; O'Brien, 2017), OT 081 (Mirzoyan, 2016a; Schüssler et al., 2017), 1RXS J023832.6-311658 (Gaté et al., 2017), and S4 0954+65 (Mirzoyan, 2015a; MAGIC Collaboration et al., 2018b). OJ 287 was within the most promising candidate list. The other three sources had a predicted VHE gamma-ray flux a bit lower than the typical sensitivity of current generation of IACTs, which we used as borderline, and therefore were not in our candidate list. However, the observed fluxes were in agreement with the predicted flux range from our method.

4.2 New discoveries at VHE gamma rays

As discussed in previous section, some of the TeV BL Lac candidates reported in Paper I were observed at VHE gamma rays. In the following sections, we will discuss the outcome of the observations of three of those sources, in which the author of this thesis had major role in requesting the observations, analysing the data, and interpreting the results. These three sources are S2 0109+22, TXS 0210+515, and 1ES 2037+521.

4.2.1 S2 0109+22

The first of the candidates which we followed with MAGIC observations was S2 0109+22. It was not among our highest ranked candidates, but was flaring in the HE gamma-ray band in July 2015, which triggered ToO observations with MAGIC telescopes. Owen & Mufson (1977) measured a strong millimetre emission from the location of S2 0109+22 (RA=01h12m06s and DEC=+22d44m39s, J2000) and identified the source as BL Lac object. Being a relatively bright ISP BL Lac object in radio and optical bands (Ciprini et al., 2003; Hovatta et al., 2008, 2014a), S2 0109+22 has been monitored since 1976.

Ciprini et al. (2004) modelled the broadband SED of the source using an extensive sample of radio and optical data together with the X-ray data

Table 4.1: The fifteen most promising TeV candidates introduced in Paper I. The last column shows whether they are detected at VHE gamma rays.

Source name	Redshift	Class.	Rank	TeV?
TXS 0149+710	0.022	HSP	1	
3C 371	0.046	ISP	2	
PKS 1252-441	0.041	LSP	3	
CRATES J061733.67-171522.8	0.098	ISP	4	
TXS 0210+515	0.049	HSP	5	Y
PMN J0444-6014	0.097	HSP	6	
PKS 2316-423	0.054	HSP	7	
1RXS J195815.6-301119	0.119	HSP	8	
1ES 2037+521	0.053	HSP	9	Y
PKS 0829+046	0.174	LSP	10	
RX J1057.8-2753	0.091	ISP	11	
OJ 287	0.306	LSP	12	Y
B2 1811+31	0.117	ISP	13	
MG1 J125348+0326	0.066	HSP	14	
4C +42.22	0.059	HSP	15	

obtained by *ROSAT* (Neumann et al., 1994) and an upper limit of gamma-ray emission from observation performed by *EGRET* (Ciprini et al., 2004). They suggested that the HE gamma-ray emission of the source would be detectable by (then) next generation of gamma-ray space telescopes, based on the brightness of the source in millimetre wavelengths and the location of its synchrotron peak frequency. During the first three-month sky-survey operation of the *Fermi*-LAT, the source was detected in HE gamma-ray band (Abdo et al., 2009) and has been listed as variable BL Lac object in most of the *Fermi*-LAT catalogues (1FGL, Abdo et al. 2010a; 2FGL, Nolan et al. 2012; 1FHL, Ackermann et al. 2013; 3FGL, Acero et al. 2015).

The first estimation of the source distance was reported by Healey et al. (2008), $z = 0.265$. However, this redshift measurement was later

disfavoured by Paiano et al. (2016) who claimed the redshift lower limit of the source $z > 0.35$, based on a high signal-to-noise optical spectrum and assuming that the source is hosted by a massive elliptical galaxy. The predicted (median) VHE gamma-ray integral flux over 200 GeV was $F_{(>200\,\mathrm{GeV})} = 1.2 \times 10^{-12}$ erg cm^{-2} s^{-1}(Paper I), which was slightly above the sensitivity limit of MAGIC telescopes (Aleksić et al., 2016).

Triggered by HE gamma-ray flux enhancement (two times higher than the average flux reported in the 3FGL catalogue) on July 20$^{\mathrm{th}}$, 2015, (MJD 57223), MAGIC telescopes observed the source between July 22$^{\mathrm{nd}}$ and 28$^{\mathrm{th}}$, 2015 (MJD 57225–57231) in seven consecutive nights with a total exposure time of 9.63 h. The discovery of the source at VHE gamma rays was announced on July 26$^{\mathrm{th}}$, 2015, after 5.3 h of data collection (Mirzoyan, 2015b). A temporal and spectral analysis of MWL data are performed in order to characterise VHE gamma-ray behaviour of the source.

The source was detected at VHE gamma rays with a significance level of 5.3σ, where the $\geq 61\%$ of excess events were collected during 1.42 h of observation on July 25$^{\mathrm{th}}$, 2015, (MJD 57228). The constant VHE gamma-ray integral flux hypothesis was disfavoured at a level of confidence of $2.65\,\sigma$ significance, indicating a flux variability with a daily timescale (Paper II). Comparing the VHE gamma-ray integral flux ($F_{>200\,\mathrm{GeV}}$) of S2 0109+22 to that of other variable TeV BL Lac objects presented in Paper I showed that both lowest and highest observed flux of S2 0109+22 are among the faintest of the population (Paper II, Fig. 3). Moreover, the highest observed flux on July 25$^{\mathrm{th}}$, 2015, is in good agreement with the highest predicted flux reported in Paper I ($F^{\mathrm{high\ obs}}_{>200\,\mathrm{GeV}} = (4.6 \pm 1.5) \times 10^{-12}$ vs. $F^{\mathrm{high\ pred}}_{>200\,\mathrm{GeV}} = (4.5 \pm 1.9) \times 10^{-12}$ erg cm^{-2} s^{-1}).

The VHE gamma-ray spectrum of the source was produced taking into account two sets of data, in order to take into account the variability of the source at VHE gamma rays. One data set only included the 1.42 h observation during the high state night (MJD 57228) while the average data from all of the VHE gamma-ray observations are included in the second data set. Excluding the high state night led to the non-detection of the source at VHE gamma rays (Paper II, Fig. 1) which prevented the reconstruction of the spectrum. We found that both the observed and the intrinsic VHE gamma-ray spectrum of the source can be described by a power law function (Eq. 3.1) despite the difference in the data sets. While the spectral index of the two data sets were compatible with each other, the flux normalisation differed. This was consistent with the VHE gamma-ray flux variability

amplitude (Paper II).

As the redshift of the source was uncertain, we performed a study to constrain it using the VHE gamma-ray spectrum of the source. Assuming that the intrinsic spectrum of the source is described by a power law or a concave function and the source is not located at $z > 1$, the absorption of VHE gamma rays through interaction with EBL can be used to probe a limit on the distance of the blazars (Mazin & Goebel, 2007; Prandini et al., 2010).

For the case of S2 0109+22, we assumed that the intrinsic spectrum of the source can be described by a power law. We tested two different values for the spectral index of the source intrinsic spectrum. The assumed spectral indexes are 1.5 and 1.81 ± 0.14. The former value was based on a conservative assumption that the spectrum of the gamma-rays emission is expected to be softer than 1.5 under most circumstances (Aharonian et al., 2006; Meyer et al., 2012). The later assumption is based on the HE gamma-ray observations obtained by *Fermi*-LAT during the MAGIC discovery campaign. Moreover, the systematic uncertainty of the instrument was taken into account via changing the simulated total light throughput of the instrument by $\pm 15\%$. Furthermore, the effect of using different EBL models were studied by assuming eight different EBL models (i.e. Franceschini et al., 2008; Kneiske & Dole, 2010; Finke et al., 2010; Gilmore et al., 2012; Helgason & Kashlinsky, 2012; Inoue et al., 2013; Stecker et al., 2016). Performing a redshift scan we obtained a 95% confidence level limit to the S2 0109+22 redshift of $z \leq 0.67$ following the method described by Rolke & López (2001). The upper-limit obtained from VHE gamma-ray data was consistent with the optical constrains (Paper II, Sec. 3.5.1).

4.2.2 TXS 0210+515 and 1ES 2037+521

EHBLs are a new emerging subclass of BL Lac objects. Their synchrotron peak is located above 10^{17} Hz, while their IC peak generally lies in the energy range above 100 GeV. This makes them promising candidates for VHE gamma-ray observations. However, compared to the HSPs they are relatively faint and the number of TeV EHBLs is still small (Costamante et al., 2018). Aiming at increasing the number of TeV EHBLs, MAGIC telescopes observed 10 targets with a total exposure time of 145 h since 2010. Among these 10 objects, TXS 0210+515 and 1ES 2037+521 were proposed as promising EHBL TeV candidates for VHE gamma-ray observations based

on the method described in Paper I.

TXS 0210+515 (RA=02h14m18s and DEC=+51d44m52s, J2000) was classified as a BL Lac object at redshift z=0.049 (Marcha et al., 1996). Its synchrotron peak is located at $\nu_{\rm synch} \geq 10^{17}$ Hz (Chang et al., 2017). We investigated the X-ray spectrum of the source in the energy range between 0.5 and 79 keV using simultaneous *Swift*-XRT and *NuSTAR* observations. We found that the synchrotron peak of the source is located at $\nu_{\rm synch} = (1.7 \pm 0.3) \times 10^{18}$ Hz (Paper III).

MAGIC telescopes observed the source for $\sim$ 29 h between 2015 and 2017. The VHE gamma-ray observations led to the detection of a signal with 5.9σ confidence level and constant VHE gamma-ray integral flux $F^{\rm obs}_{>200\,\rm GeV} = (1.6 \pm 0.5) \times 10^{-12}\,\rm cm^{-2}\,s^{-1}$ (Paper III). The observed flux is in good agreement with the minimum predicted flux $F^{\rm min\ pred}_{>200\,\rm GeV} = 2.0 \times 10^{-12}\,\rm cm^{-2}\,s^{-1}$ reported in Paper I. The intrinsic VHE gamma-ray spectrum of the source can be described as a power-law model (Eq. 3.1) with a photon index of $\Gamma_{\rm VHE} = 1.6 \pm 0.3$ in the energies between 500 and 1500 GeV. The hard photon index at VHE gamma rays indicates that the IC peak of the SED is located at ranges above 1 TeV (see Sec. 4.3 for more details).

Véron-Cetty & Véron (2006) classified 1ES 2037+521 (RA=20h39m24s and DEC=+52d19m50s, J2000) as a BL Lac object, and it is located at z=0.053 (Nilsson et al., 2003). The location of its synchrotron peak was unclear due to the contribution of the host-galaxy to the optical flux (Paper I) and led it to be dropped out from most candidate selection procedures. Further investigation of its X-ray behaviour, using multiple observations performed by *Swift*-XRT, showed that its X-ray photon index in the range of 1.5 and 10 keV is always below or consistent with the EHBL candidate criteria of $\Gamma_X \leq 2.0$ (Paper III). This is an indication of the synchrotron peak of the source to be above 10^{17} Hz.

MAGIC observations in September 2016 (exposure time=11 h) confirmed the first detection of VHE gamma-ray signal with 5.7σ confidence level and VHE gamma-ray integral flux $\sim$ 3% of the flux of the Crab nebula above 200 GeV (Mirzoyan, 2016b). Further VHE gamma-ray observations revealed that the spectrum of the source can be described by power-law model (Eq. 3.1) with the intrinsic photon index of $\Gamma_{\rm VHE} = 2.0 \pm 0.5$ and constant VHE gamma-ray integral observed flux of $F^{\rm obs}_{>200\,\rm GeV} = (3.0 \pm 0.5) \times 10^{-12}\,\rm cm^{-2}\,s^{-1}$ (Paper III). The observed flux was $\sim$ 2 times higher than the minimum predicted flux ($F^{\rm min\ pred}_{>200\,\rm GeV} = 1.5 \times 10^{-12}\,\rm cm^{-2}\,s^{-1}$) reported

in Paper I.

In these two cases the intrinsic VHE gamma-ray spectrum is in agreement with the hypothesis of being hard-TeV EHBLs ($\Gamma_{\rm vhe,int} \leq 2.0$). Both cases are included in the mini-catalogue of EHBLs along with nine other sources (Paper III). Within the promising candidates listed in Paper I, three more objects are possible EHBLs based on the current available data in lower energy bands. These three sources are RX J0805.4+7534, TXS 0652+426, and MS 0737.9+7441 which can be detected in VHE gamma-ray band in less than 30 hours of observation.

4.3 Spectral energy distribution

In this thesis work we applied several different models, two of them were described in Section 3.6. These two models were a spherical single-zone SSC model and an observationally-constrained two-component model which were used in Paper II and Paper IV, respectively.

In Paper II, the single-zone SSC model described the broadband SED well. The emission region size was compatible with a variability timescale of 24 hours, in our model. The lowest frequencies (below millimetre band) were not reproduced by the model. The emission in radio is generally assumed to be produced in the outer region of the jet. This was in agreement with the model setup in which the emission region was located near to the central engine and the effect of synchrotron self-absorption was strong. Moreover, this result was consistent with the results in Section 3.4, where we did not find any connection between radio and optical light curves of S2 0109+22.

A hint of ISP to HSP transition is found when comparing the SED of S2 0109+22 presented in Paper II with archival data. Such a transition had been previously suggested for other TeV BL Lac objects (se e.g. H.E.S.S. Collaboration et al., 2013; Ahnen et al., 2016a). The parameters of the single-zone SSC model were rather typical for TeV BL Lac objects (see e.g. Tavecchio et al., 2010). The strength of the magnetic field in our model was an order of magnitude weaker than the ones reported by Ciprini et al. (2004) who did not use VHE gamma-ray data. Therefore, lower magnetic field strength was needed, because, in order to reproduce the observed VHE gamma-ray emission (i.e. higher SSC luminosity), the ratio between radiation and magnetic energy had to be increased.

The first systematic attempt to model the broadband SEDs of TeV BL Lacs using an observationally-constrained two-component model were presented in Paper IV. In our model, we investigated the case where the two co-spatial interacting regions were located close to the VLBI core. The model was used to reproduce the SED of eight MWL data sets of five TeV BL Lac objects (see Sec. 3.1 on how these sources were selected). We took into account all of the observational constraints from VLBI data. The main results of our modelling can be summarised as follows:

- In our model, and for all of the studied cases, the emission in X-ray to VHE gamma-ray bands was dominated by the emission from the blob while the emission from core dominated the radio band. Considering the core component in our model had two major outcomes. On one hand, as the two components were assumed to be co-spatial, the seed photons provided by the core component for the Compton scattering relaxed the requirement of a very low strength of magnetic field and high Doppler factors for the blob component, which are usually required by one-zone SSC models. On the other hand, the core component put constraints on the flux of low energy part of blob component as it always extended to the optical band (Paper IV, see Fig. 8).

- Typical SED parameters of one-zone SSC models for TeV BL Lac objects are usually far from equipartition, i.e. the energy carried by the magnetic field is several orders of magnitude lower than the kinetic energy of the particles Tavecchio & Ghisellini (2016). The SED parameters in our two-component model suggested solutions close to equipartition for the entire core and blob system in all of the cases. The energy carried by magnetic field slightly dominating over the kinetic energy of the particles except for one case (Paper IV, see Tab. 7).

- Our sample includes three HSPs and two ISPs. Even our sample is not conclusive, we found that the used parameters in SED modelling were similar between the three HSPs and the two ISPs (Paper IV, see Tab. 6). Moreover, our sample SEDs represented different types of TeV BL Lac objects during both quiescent and flaring states. This indicates that the observationally-constrained two-component model should be applicable to a wide range of TeV BL Lac objects.

- In our model, the emission regions were located at the VLBI core. It was possible to reproduce the SEDs with Doppler factors and magnetic field strengths values, which were in agreement with the results of VLBI observations. This demonstrated that the radio component, which is usually neglected in a one-zone SSC scenario, does not have to originate from a region far away from the region which was responsible for X-ray and VHE gamma-ray emission.

One of the aims of Paper III was investigating the broadband SED of hard-TeV EHBLs. Being a new emerging class of TeV BL Lac objects, the SED of the EHBLs has not been studied systematically. Therefore, three different models were used to perform a systematic investigation. The SED of all of the eleven objects in the sample of Paper III were modelled using single-zone conical jet SSC model described by (Asano & Hayashida, 2018). Six of the objects which had a VHE gamma-ray spectra determination were also modelled using a two-zone spine-layer SSC model (Tavecchio & Ghisellini, 2008) and a proton synchrotron model (Cerruti et al., 2015). All models described the MWL observational data very well. However, the resulting parameters of the models were different. In particular, the single-zone conical jet SSC model led to very low magnetisation. I.e. the ratio between the energy carried by magnetic field to the kinetic energy of the particles were as low as 10^{-3}.

The two-zone spine-layer SSC model resulted in quasi-equipartition and solved the magnetisation problem. The estimated jet powers in this scenario were an order of magnitude lower than those required by the single-zone conical jet SSC model. Application of the proton synchrotron model resulted in a highly magnetised jet which was far from equipartition. Therefore, with the current data set we cannot favour or disfavour any of the considered models. Studying the correlation between X-ray and VHE gamma-ray flux is the most powerful tool available to discriminate between models. But comparing the VHE gamma-ray flux of these source with the sensitivity of current generation of IACTs, this is mostly a target for telescopes of the future generation (see Fig. 4.1).

4.4 Summary of the results

In this thesis, we have investigated TeV BL Lac objects. They are the most numerous objects in the VHE gamma-ray sky, but still only ~ 65 of them

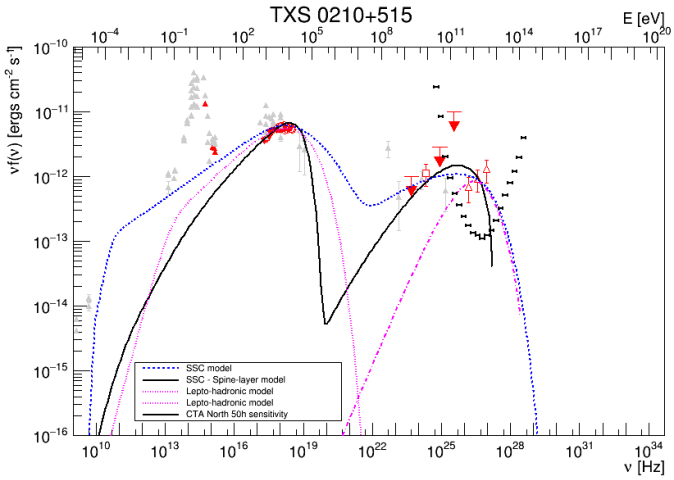

Figure 4.1: The SED of TXS 0210+515. The black points show the differential sensitivity of the CTA north array for 50 h of observation at a zenith distance of 20° . The figure is adopted from Paper III. Image credit: Elisa Prandini.

are known and the population is far from complete. Also, it is difficult to explain their observed variability, polarisation behaviour and SED within current emission models.

Aiming at increasing the number of the BL Lac objects in VHE gamma-ray sky, we developed an empirical MWL prediction method and introduced a list of 53 TeV BL Lac candidates from which nine of them have high enough predicted VHE gamma-ray flux to be detectable in less than 25 h of observation with the third generation of IACTs (Paper I).

We also followed many of these candidates with dedicated studies of their MWL variability and spectral energy distribution. The first source that we studied was an intermediate BL Lac object (S2 0109+22). We found that the source is variable in the VHE gamma-ray band and a spherical single-zone SSC model can describe the broadband SED of the source very well. Moreover, we did not find any connection between the radio and optical light curves of the source. When compared to the larger sample of BL Lac objects, the polarisation behaviour of the source was rather typical for ISP sources (Paper II).

Some of the candidates identified in Paper I showed spectral characteristics of the EHBLs. Two of them (TXS 0210+515 and 1ES 2037+521) were proposed for VHE gamma-ray observation by the author of this thesis. The VHE gamma-ray observation resulted in the discovery of these two source at VHE gamma rays. Moreover, we found that these two sources exhibited all signatures to be categorised as hard-TeV EHBLs. Furthermore, the SEDs of the sources were modelled using three different scenarios. However, more simultaneous MWL observations are needed to fully characterise the SEDs of the sources. Especially the hard X-ray emission of 1ES 2037+521 has to be investigated thoroughly, as currently no observations are available in this energy range (Paper III).

Finally we performed an extensive study of observationally-constrained two-component modelling of TeV BL Lac objects. In this model, the two-components were co-spatial and located at the VLBI core. The observational constraints were obtained from VLBI data, optical polarisation, and long-term light curves (radio, optical, and X-rays) to limit the parameter space. The model was tested on five TeV BL Lac objects (2 ISP and 3 HSP) during both flaring and low state. Therefore, the observationally-constrained two-component model should be applicable to a wide range of TeV BL Lac objects. We found that the usually ignored radio emission in one-zone SSC models does not have to originate from a region far away from the region which was in charge of X-ray and VHE gamma-ray emission (Paper IV).

Bibliography

Abdalla H., et al., 2019, Nature, 575, 464

Abdo A. A., et al., 2009, ApJ, 700, 597

Abdo A. A., et al., 2010a, ApJS, 188, 405

Abdo A. A., et al., 2010b, ApJ, 716, 30

Abdo A. A., et al., 2010c, ApJ, 716, 30

Acciari V. A., et al., 2011, ApJ, 738, 25

Acciari V. A., et al., 2020, ApJS, 247, 16

Acero F., et al., 2009, Science, 326, 1080

Acero F., et al., 2015, ApJS, 218, 23

Acero F., et al., 2016, ApJS, 223, 26

Ackermann M., et al., 2013, ApJS, 209, 34

Aharonian F. A., 2000, NewA, 5, 377

Aharonian F., et al., 2006, Nature, 440, 1018

Ahnen M. L., et al., 2015, ApJ, 815, L23

Ahnen M. L., et al., 2016a, MNRAS, 459, 2286

Ahnen M. L., et al., 2016b, A&A, 595, A98

Ahnen M. L., et al., 2017a, MNRAS, 468, 1534

Ahnen M. L., et al., 2017b, MNRAS, 472, 2956

Ajello M., et al., 2017, ApJS, 232, 18

Akritas M. G., Siebert J., 1996, MNRAS, 278, 919

Albert J., et al., 2008, Nuclear Instruments and Methods in Physics Research A, 588, 424

Aleksić J., et al., 2014, A&A, 567, A135

Aleksić J., et al., 2015, A&A, 576, A126

Aleksić J., et al., 2016, Astroparticle Physics, 72, 76

Aliu E., et al., 2014, ApJ, 797, 89

Angel J. R. P., Stockman H. S., 1980, ARA&A, 18, 321

Angelakis E., et al., 2016, MNRAS, 463, 3365

Ansoldi S., et al., 2018, ApJ, 863, L10

Arsioli B., et al., 2015, A&A, 579, A34

Asano K., Hayashida M., 2018, ApJ, 861, 31

Barres de Almeida U., et al., 2010, MNRAS, 408, 1778

Barres de Almeida U., Tavecchio F., Mankuzhiyil N., 2014, MNRAS, 441, 2885

Beckmann V., Shrader C., 2012, in Proceedings of "An INTEGRAL view of the high-energy sky (the first 10 years)" - 9th INTEGRAL Workshop and celebration of the 10th anniversary of the launch (INTEGRAL 2012). 15-19 October 2012. Bibliotheque Nationale de France. p. 69 (arXiv:1302.1397)

Bignami G. F., et al., 1981, A&A, 93, 71

Blinov D., et al., 2016, MNRAS, 457, 2252

Bloom S. D., Marscher A. P., 1996, ApJ, 461, 657

Bonnoli G., et al., 2015, MNRAS, 451, 611

Böttcher M., 2019, Galaxies, 7, 20

Burrows D. N., et al., 2004, in Flanagan K. A., Siegmund O. H. W., eds, Proc. SPIEVol. 5165, X-Ray and Gamma-Ray Instrumentation for Astronomy XIII. pp 201–216, doi:10.1117/12.504868

Burrows D. N., et al., 2005, Space Sci. Rev., 120, 165

Cao G., et al., 2019, arXiv e-prints, p. arXiv:1912.07448

Cerruti M., 2019, arXiv e-prints, p. arXiv:1912.03666

Cerruti M., et al., 2015, MNRAS, 448, 910

Cerruti M., et al., 2017, A&A, 606, A68

Chang Y.-L., et al., 2017, A&A, 598, A17

Ciprini S., et al., 2003, A&A, 400, 487

Ciprini S., et al., 2004, MNRAS, 348, 1379

Cohen M. H., et al., 1971, ApJ, 170, 207

Costamante L., Ghisellini G., 2002, A&A, 384, 56

Costamante L., et al., 2001, A&A, 371, 512

Costamante L., et al., 2018, MNRAS, 477, 4257

Curtis H. D., 1918, Publications of Lick Observatory, 13, 9

D'Abrusco R., et al., 2014, ApJS, 215, 14

D'Elia V., et al., 2013, A&A, 551, A142

De Naurois M., 2019, The Astronomer's Telegram, 13052, 1

Dermer C. D., Schlickeiser R., 1993, ApJ, 416, 458

Dermer C. D., Murase K., Inoue Y., 2014, Journal of High Energy Astrophysics, 3, 29

Domínguez A., et al., 2011, MNRAS, 410, 2556

Drake A. J., et al., 2009, ApJ, 696, 870

Edelson R. A., Krolik J. H., 1988, ApJ, 333, 646

Efron B., Stein C., 1981, Annals of Statistics, 9, 586

Efron B., Tibshirani R. J., 1993. Chapman & Hall, New York, NY

Evans P. A., et al., 2009, MNRAS, 397, 1177

Fallah Ramazani V., Lindfors E., Nilsson K., 2017, A&A, 608, A68

Finke J. D., Razzaque S., Dermer C. D., 2010, ApJ, 712, 238

Flesch E., Hardcastle M. J., 2004, A&A, 427, 387

Fossati G., et al., 1998, MNRAS, 299, 433

Franceschini A., Rodighiero G., Vaccari M., 2008, A&A, 487, 837

Gaté F., H. E. S. S. Collaboration Fitoussi T., 2017, in 35th International Cosmic Ray Conference (ICRC2017). p. 645 (arXiv:1708.09612)

Gehrels N., et al., 2004, ApJ, 611, 1005

Ghisellini G., et al., 2017, MNRAS, 469, 255

Gilmore R. C., et al., 2012, MNRAS, 422, 3189

Goodman J., Weare J., 2010, Commun. Appl. Math. Comput. Sci., 5, 65

Gregory P. C., Condon J. J., 1991, ApJS, 75, 1011

Gregory P. C., et al., 1994, ApJS, 90, 173

Gregory P. C., et al., 1996, ApJS, 103, 427

Griffith M. R., et al., 1995, ApJS, 97, 347

H. E. S. S. Collaboration et al., 2015a, Science, 347, 406

H. E. S. S. Collaboration et al., 2015b, A&A, 573, A31

H.E.S.S. Collaboration et al., 2013, A&A, 559, A136

Harrison F. A., et al., 2013, ApJ, 770, 103

Hassan T., et al., 2017, in 35th International Cosmic Ray Conference (ICRC2017). p. 632 (arXiv:1708.07704)

Healey S. E., et al., 2008, ApJS, 175, 97

Helgason K., Kashlinsky A., 2012, ApJ, 758, L13

Hodge M. A., et al., 2018, ApJ, 862, 151

Hovatta T., et al., 2008, A&A, 485, 51

Hovatta T., et al., 2014a, AJ, 147, 143

Hovatta T., et al., 2014b, MNRAS, 439, 690

Hovatta T., et al., 2016, A&A, 596, A78

Hufnagel B. R., Bregman J. N., 1992, ApJ, 386, 473

Hughes M. P., 1965, Nature, 207, 178

Hughes P. A., Aller H. D., Aller M. F., 1989, ApJ, 341, 54

IceCube Collaboration et al., 2018, Science, 361, eaat1378

Inoue Y., et al., 2013, ApJ, 768, 197

Isobe T., et al., 1990, ApJ, 364, 104

Jones D. H., et al., 2009, MNRAS, 399, 683

Jorstad S., Marscher A., 2016, Galaxies, 4

Kalberla P. M. W., et al., 2005, A&A, 440, 775

Kneiske T. M., Dole H., 2010, A&A, 515, A19

Komin N., et al., 2012, arXiv e-prints, p. arXiv:1201.0639

Komin N., Haupt M., H. E. S. S. Collaboration 2017, in 35th International Cosmic Ray Conference (ICRC2017). p. 730 (arXiv:1708.03171)

Konigl A., 1981, ApJ, 243, 700

Landi Degl'Innocenti E., Bagnulo S., Fossati L., 2007, in Sterken C., ed., Astronomical Society of the Pacific Conference Series Vol. 364, The Future of Photometric, Spectrophotometric and Polarimetric Standardization. p. 495 (arXiv:astro-ph/0610262)

Laurent-Muehleisen S. A., et al., 1999, ApJ, 525, 127

Li T. P., Ma Y. Q., 1983, ApJ, 272, 317

Li W., et al., 2003, PASP, 115, 844

Lindfors E., MAGIC Collaboration 2012, in Journal of Physics Conference Series. p. 012003, doi:10.1088/1742-6596/355/1/012003

Lindfors E. J., et al., 2016, A&A, 593, A98

Lister M. L., Homan D. C., 2005, AJ, 130, 1389

Lister M. L., et al., 2009, AJ, 137, 3718

Lister M. L., et al., 2016, AJ, 152, 12

Lister M. L., et al., 2018, ApJS, 234, 12

Lister M. L., et al., 2019, ApJ, 874, 43

Luo J.-W., Zhang B., 2020, Phys. Rev. D, 101, 103015

Lyutikov M., Pariev V. I., Gabuzda D. C., 2005, MNRAS, 360, 869

MAGIC Collaboration et al., 2018a, MNRAS, 480, 879

MAGIC Collaboration et al., 2018b, A&A, 617, A30

MAGIC Collaboration et al., 2019, Nature, 575, 455

MAGIC Collaboration et al., Submitted, Testing two-component models on very-high-energy gamma-ray emitting BL Lac objects, A&A

MAGIC collaboration et al., 2020, arXiv e-prints, p. arXiv:2001.08678

Mannheim K., 1996, Space Sci. Rev., 75, 331

Mannheim K., Biermann P. L., 1989, A&A, 221, 211

Maraschi L., Tavecchio F., 2003, ApJ, 593, 667

Maraschi L., Ghisellini G., Celotti A., 1992, ApJ, 397, L5

Marcha M. J. M., et al., 1996, MNRAS, 281, 425

Marscher A. P., Gear W. K., 1985, ApJ, 298, 114

Massaro E., et al., 2004, A&A, 413, 489

Massaro F., et al., 2011, ApJ, 739, 73

Massaro F., et al., 2013, ApJS, 206, 13

Max-Moerbeck W., et al., 2014a, MNRAS, 445, 437

Max-Moerbeck W., et al., 2014b, MNRAS, 445, 428

Mazin D., Goebel F., 2007, ApJ, 655, L13

Meyer M., et al., 2012, A&A, 542, A59

Mirzoyan R., 2015a, The Astronomer's Telegram, 7080

Mirzoyan R., 2015b, The Astronomer's Telegram, 7844

Mirzoyan R., 2016a, The Astronomer's Telegram, 9267

Mirzoyan R., 2016b, The Astronomer's Telegram, 9582

Moharana R., et al., 2020, arXiv e-prints, p. arXiv:2002.01661

Moralejo A., et al., 2009, preprint, (arXiv:0907.0943)

Mücke A., Protheroe R. J., 2001, Astroparticle Physics, 15, 121

Mukherjee R., VERITAS Collaboration 2017, The Astronomer's Telegram, No. 10051, 51

Neumann M., et al., 1994, A&AS, 106, 303

Nilsson K., et al., 2003, A&A, 400, 95

Nilsson K., et al., 2018, A&A, 620, A185

Nolan P. L., et al., 2012, ApJS, 199, 31

O'Brien S., 2017, arXiv e-prints, p. arXiv:1708.02160

Owen F. N., Mufson S. L., 1977, AJ, 82, 776

Pacholczyk A. G., 1970. San Francisco (Calif.) : Freeman, 1970.

Padovani P., Giommi P., 2015, MNRAS, 446, L41

Paiano S., et al., 2016, MNRAS, 458, 2836

Pearson T. J., et al., 1981, Nature, 290, 365

Petropoulou M., Giannios D., Sironi L., 2016, MNRAS, 462, 3325

Piner B. G., Edwards P. G., 2004, ApJ, 600, 115

Piner B. G., Edwards P. G., 2018, ApJ, 853, 68

Piner B. G., Pant N., Edwards P. G., 2008, ApJ, 678, 64

Piner B. G., Pant N., Edwards P. G., 2010, ApJ, 723, 1150

Prandini E., 2011, PhD thesis, Padua U., http://paduaresearch.cab.unipd.it/3757/

Prandini E., et al., 2010, MNRAS, 405, L76

Pushkarev A. B., et al., 2012, A&A, 545, A113

Rees M. J., 1966, Nature, 211, 468

Rees M. J., 1967, MNRAS, 135, 345

Richards J. L., et al., 2011, ApJS, 194, 29

Rolke W. A., López A. M., 2001, Nuclear Instruments and Methods in Physics Research A, 458, 745

Sanchez D. A., Deil C., 2013, in International Cosmic Ray Conference. p. 2784 (arXiv:1307.4534)

Schmidt M., 1963, Nature, 197, 1040

Schreier E. J., Gorenstein P., Feigelson E. D., 1982, ApJ, 261, 42

Schultz C., 2013, PhD thesis, Padua U., https://magic.mpp.mpg.de/backend/publication/show/22

Schüssler F., et al., 2017, in 35th International Cosmic Ray Conference (ICRC2017). p. 652 (arXiv:1708.01083)

Stecker F. W., Scully S. T., Malkan M. A., 2016, ApJ, 827, 6

Stroh M. C., Falcone A. D., 2013, ApJS, 207, 28

Takalo L. O., et al., 2008, in Aharonian F. A., Hofmann W., Rieger F., eds, Vol. 1085, American Institute of Physics Conference Series. pp 705–707, doi:10.1063/1.3076774

Tavecchio F., Ghisellini G., 2008, MNRAS, 385, L98

Tavecchio F., Ghisellini G., 2016, MNRAS, 456, 2374

Tavecchio F., Maraschi L., Ghisellini G., 1998, ApJ, 509, 608

Tavecchio F., et al., 2010, MNRAS, 401, 1570

Teräsranta H., et al., 1998, A&AS, 132, 305

Terzić T., 2015, PhD thesis, University of Zagreb, https://repozitorij.pmf.unizg.hr/en/islandora/object/pmf%3A1656

Tiet V. C., Piner B. G., Edwards P. G., 2012, arXiv e-prints,

VERITAS Collaboration et al., 2009, Nature, 462, 770

Valtaoja L., et al., 1989. Springer US, p. 127, doi:10.1007/BFb0031153

Valtaoja L., et al., 1991, AJ, 101, 78

Véron-Cetty M. P., Véron P., 2006, A&A, 455, 773

Villforth C., et al., 2010, MNRAS, 402, 2087

Voges W., et al., 1999, A&A, 349, 389

Wagner R. M., 2008, MNRAS, 385, 119

Wakely S. P., Horan D., 2008, in International Cosmic Ray Conference. pp 1341–1344

Weekes T. C., et al., 1989, ApJ, 342, 379

Welsh W. F., 1999, PASP, 111, 1347

Wood M., et al., 2017, in 35th International Cosmic Ray Conference (ICRC2017). p. 824 (arXiv:1707.09551)

Wright E. L., et al., 2010, AJ, 140, 1868

Zanin R., et al., 2013, in Proceedings of the 33rd International Cosmic Ray Conference (ICRC2013): Rio de Janeiro, Brazil, July 2-9, 2013. p. 0773, http://inspirehep.net/record/1412925/files/icrc2013-0773.pdf

Author's contributions to the publications

Paper I

The author collected all data, performed the statistical correlation analyses, and invented the prediction method. The author was the corresponding author of the paper.

Paper II

The author analysed the X-ray, VHE gamma-ray, and optical polarisation data. The author also collected all of the MWL data. The author was corresponding author of the paper on behalf of MAGIC collaboration.

Paper III

The author was involved in the project from the beginning, actively participating in selection of sources for the VHE gamma-ray observation proposal. The author analysed the X-ray and part of the VHE gamma-ray data. The author participated in the interpretation of the data and was one of the corresponding authors of the paper.

Paper IV

The author analysed the X-ray data, optical polarisation, and part of VHE gamma-ray data. The author also collected the majority of MWL data and modelled the SED of the sources. The author was corresponding author of the paper on behalf of MAGIC collaboration.